AD 414486

63-4-5

ASD-TDR-63-461

STUDY OF ELECTRON FOCUSING BY NON-LINEAR SPIRALS

Technical Documentary Report No. ASD-TDR-63-461

May 1963

Air Force Avionics Laboratory
Electronic Technology Division
Aeronautical Systems Division
Air Force Systems Command
Wright-Patterson Air Force Base, Ohio

Project No. 4156, Task No. 415605

(Prepared under Contract AF 33(657)-7682)

PICKUP TUBE OPERATION
POWER TUBE DEPARTMENT
GENERAL ELECTRIC
Syracuse, N. Y.

NOTICES

When Government drawings, specifications, or other data are used for any purpose other than in connection with a definitely related Government procurement operation, the United States Government thereby incurs no responsibility nor any obligation whatsoever; and the fact that the Government may have formulated, furnished, or in any way supplied the said drawings, specifications, or other data, is not to be regarded by implication or otherwise as in any manner licensing the holder or any other person or corporation or conveying any rights or permission to manufacture, use, or sell any patented invention that may in any way be related thereto.

Qualified requesters may obtain copies of this report from the Armed Services Technical Information Agency, (ASTIA), Arlington Hall Station, Arlington 12, Virginia.

This report has been released to the Office of Technical Services, U. S. Department of Commerce, Washington 25, D. C., for sale to the general public.

Copies of this report should not be returned to the Aeronautical Systems Division unless return is required by security considerations, contractual obligations, or notice on a specific document.

FOREWORD

This report was prepared by the Pickup Tube Operation of the Power Tube Department, General Electric Company, Syracuse, New York, on Air Force Contract AF 33(657)-7682, under Task No. 415605 of Project No. 4156 entitled "Electronic Tube Technology".

The studies presented began in February 1962 and were completed in March 1963. Dr. Kurt Schlesinger was project engineer for the General Electric Company while Elgene R. Nichols and Raymond C. Rang were successive project engineers for Aeronautical Systems Division*.

Other major contributors and their fields of interest were:

L. Heuschneider - Titanium oxide films

W. J. Noroski - Fine-grain phosphors for image tubes

J. E. Roderick - Photocathode processing and manufacturing

R. Wagner - Mechanical and electrical engineering (including the development of tools for spiral manufacturing) and glass- and vacuum-technology

J. Wilburt - Construction of spiral lenses and of electrical accessories

Section 7, Processing Techniques, was written by Mr. J. E. Roderick, Senior Development Engineer, Pickup Tube Operation Engineering.

This report is the final report, and it concludes the work on Contract AF 33(657)-7682.

*Electronic Technology Division of Air Force Avionics Laboratory

ABSTRACT

The purpose of the research work was to develop an electrostatic image converter with the following capabilities:

1. Electrostatic image formation between two plane surfaces.
2. Control of electronic magnification by spiral-lens elements.
3. Development of reflective electron-optics for image formation from photoconductive targets.

Items 1 and 2 have been accomplished. Item 3 had to be discontinued at contract termination after an electron image from a simulated non-emissive target had been demonstrated.

Early experiments used a thermionic analog. This consisted of a perforated 3" metal plate, which was illuminated by a collimated floodbeam at controlled voltage.

The built-in field-lens problem was attacked first by a ray-tracing analysis. This suggested the use of a convex mesh, close to cathode. Although image quality was disappointing, the tests verified the need for a convex, rather than a concave, shape of the mesh.

Next, the functions of first-anode and field-flattening were separated. This led to a two-mesh field-lens of the plano-convex type. This structure was retained for the remainder of the contract.

As an alternative, the balancing of aberrations in a lens doublet was investigated and was found to be operational.

A first sealed-off image tube with fixed magnification, using one spiral lens, was built and gave good results.

An analysis by Electron Trigonometry indicated feasibility of controlling magnification over a 7:1 range. A sealed-off Zoom tube, using two spirals in tandem, yielded a Zoom-range of 4.5-to-1 between planes. This tube also functions as a stop-motion switch and permits independent control of display intensity by ultor voltage.

ABSTRACT (Continued)

Toward the end of contract, two tests with reflective electron optics were made. The second test resulted in a 1-to-1 electron-image from a voltage-controlled, simulated target. A 1-to-1 image with fair resolution (30 lines per inch) was obtained and was fully controlled by 30 volts on target.

PUBLICATION REVIEW

Publication of this technical documentary report does not constitute Air Force approval of the report's findings or conclusions. It is published only for the exchange and stimulation of ideas.

WILLIAM H. NELSON
Chief, Sensor and Display Section
Electronic Technology Division

TABLE OF CONTENTS

TABLE OF CONTENTS (Continued)

LIST OF ILLUSTRATIONS

LIST OF ILLUSTRATIONS (Continued)

LIST OF ILLUSTRATIONS (Continued)

LIST OF TABLES

INTRODUCTION

The art of image tubes is approaching its 30th anniversary. It was in 1934 that Holst et al at Philips demonstrated the conversion from an infrared into a visible image, using electron-optics to supply the balance of power.[1] This early tube took a simple "contact-print" of the subject image; i.e., it used the properties of a non-focusing electrostatic (e-s) field between closely spaced planes.

This fundamental work soon was followed by Zworykin, Morton, and Ramberg, who introduced e-s lenses with cylindrical geometry.[2,3,4] In these systems, curvature-of-field is a serious aberration. In their basic papers of 1936[2,3], Zworykin and Morton demonstrated the usefulness of a curved-cathode surface. This has become a characteristic feature of e-s image tubes to this day.[5]

The point-centered, or spherical, e-s field came later. It was introduced in 1952 by Schagen et al, who presented a detailed analysis of image formation between spherical surfaces.[6] The spherical-field approach has found wide acceptance, because of its inherent simplicity and its ability to operate from a single voltage.[7] However, the spherical, rather than plane, shape of the cathode surface had to be continued. Strictly speaking, the image surface should be curved also.

At about the same time (1953), Francken demonstrated that a mesh-anode near cathode is compatible with electron-optics of high resolution.[8] This technique introduced image converters into the field of high-speed photography[9]. This trend was continued by Linden[10], who placed a concentric spherical mesh close behind the spherical cathode for the combined purpose of stop-motion operation and of vernier focusing.

Variable magnification had been a desirable objective ever since Zworykin had demonstrated, in 1936, the flexibility of size in image converters.[2] Responding to the needs of TV broadcasting, Francken et al[8,11] developed, in 1953, a magnetic image section with a 2:1 range continuous Zoom, using a multi-section, non-rotating coil to focus.

Ten years later, Schagen announced an electrostatic Zoom lens at a 1962 convention of the IRE.[12] His work happened to coincide with developments already going on at General Electric under the subject contract.

In 1958, Baker and Papp[13] compared the relative merits of electrostatic-vs.-magnetic image converters. The latter were found to be greatly superior in focus uniformity and smaller in size. As an added advantage, the electromagnetic (e-m) system uses a plane, rather

Manuscript released by the author on June 28, 1963, for publication as an ASD technical documentary report.

than a curved, photocathode. This makes the e-m tube compatible with standard photographic objectives.

At the present time, a re-appraisal is under way in various laboratories to determine the practical utility of either system. Such re-appraisal has to take into account many factors, including not only performance ultimates but also power supply, size, and weight. The latter may include such ancillary optical equipment as field correctors and perhaps optical Zoom lenses.

Viewed against this general background, the technical study ordered by the sponsoring agency (Contract AF 33(657)-7682, 26 February 1962 to 26 March 1963) may be a timely one. This may be a "last call" to disclose potentialities of the e-s system that may not have been exploited fully in the past. It is hoped that the results to be reported may contribute something in this direction.

1. THE SPIRAL-LENS COMPONENT

A. Square-Law Type of Winding and Its Approximations

Spiral-optics, as used in the subject contract, employs cylindrical spiral-lenses as components for electron-optical systems. Glass cylinders, coated with resistive spirals, will exhibit electron-lens effects, provided that radial force components, which are proportional to radius everywhere within the volume enclosed, are set up. This hyperbolic lens field comes into being only if the axis potential follows a square law. This is accomplished by enforcing a similar voltage distribution on the inside wall of the cylindrical envelope. In addition, it is often, but not always, necessary to provide conductive terminations for the spiral cylinder. These may take the form of apertured discs or of curved meshes of high transmission, shaped as required by the electron-optical problem at hand.

In practice, it is difficult to realize a voltage-drop on a cylinder-wall, which strictly observes a square-law relationship with the axis-coordinate (z). To do so, the turn-density n, i.e., the number of turns per (axial) inch, should vary as a linear function of z. This would require a spindle-lathe with programmed gear-ratio.

1. Two-Step Approximation

Fortunately, it is possible to achieve a very good approximation to the square-law function by meeting it with two selected tangents. In each of these two sections or "steps", the turn density has a constant value. This two-step approximation is illustrated in Figure 1.1

Figure 1.1-a shows a square-law distribution of axis potential V with vertex at A. This curve is well-met by two tangential segments BC and CD. Points B and C lie at 1/4 and 3/4 respectively of the total length ℓ of the unit, which also includes a conductive band from A to B, measuring 1/4 ℓ.**

Since the ordinate of point C is halfway up on the voltage scale, we arrive at once at the spiral-lens winding as shown in Figure 1.1-b. This winding employs two "constant-n" types of spiral sections, the first being twice

** Since this band can be considered as another "step" with a turn-density of n = 1, the non-linear spiral as shown in Figure 1.1a and 1.1b is actually a three-step, rather than a two-step, approximation to the ideal square-law.

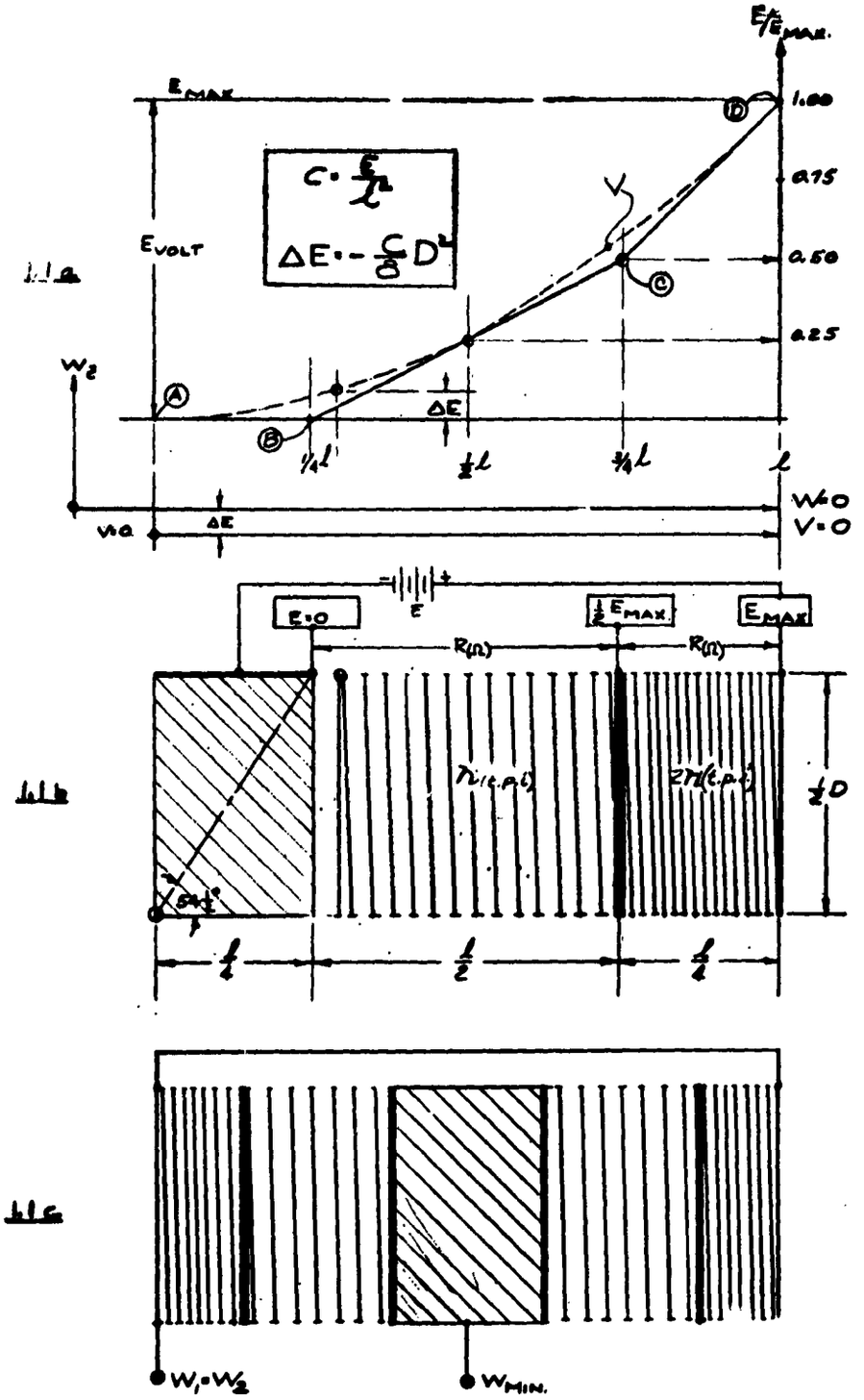

fig. 1.1 - SPIRAL LENS DESIGN: TWO-STEP APPROXIMATION

1. THE SPIRAL-LENS COMPONENT (Continued)

as long as the second and having twice the pitch. Both thus have the same total number of turns, but the second short spiral has twice the turn density n of the first as measured in turns per axial inch.

Figure 1.1-c shows a non-accelerating spiral lens that is being used in the image tubes to be reported below. This lens is essentially a combination of two units, as shown in 1.1-b, mounted back-to-back. This type of lens is used as the main focusing element in the "fixed-m" -type of image converters, described in Section 4.

A more advanced type of spiral-lens is shown in Figure 1.2. This is a non-accelerating spiral-lens doublet. It is being used successfully as a Zoom-lens in a new type of image converter, with variable magnification, which is described in more detail later in this report (Section 5).

2. One-Step Approximation

In many practical applications, the two-step approximation to a square-law (Figure 1.3-a) has been found to be better than necessary. A simpler approximation, using only one tangent to the ideal spiral, often does the job. Figure 1.3-b illustrates this for a non-accelerating, symmetrical spiral-lens. Here, the total length is sub-divided into thirds, with the first and third sections wound at constant pitch, while the center band is reserved for focusing.

This one-step approximation to non-linearity has been used successfully in many devices, including beam tubes, and even Zoom-lenses. An example for the latter is drawn up in Figure 1.3-c.

Next, we turn to a more-detailed discussion of helix-design and manufacture.

B. The Spiral as a Circuit Element

1. Equivalent Network

The use of resistive spirals with controlled distribution of turn density is becoming increasingly important in electron optics. These spiral units are used as a low-impedance type (2-to-5 megohms) and as a high-impedance type (20-to-50 megohms). These are used respectively at low-voltage levels (1-2 KV) and at very high voltages (10-to-20 KV), and with power dissipation not exceeding 2 watts per unit.

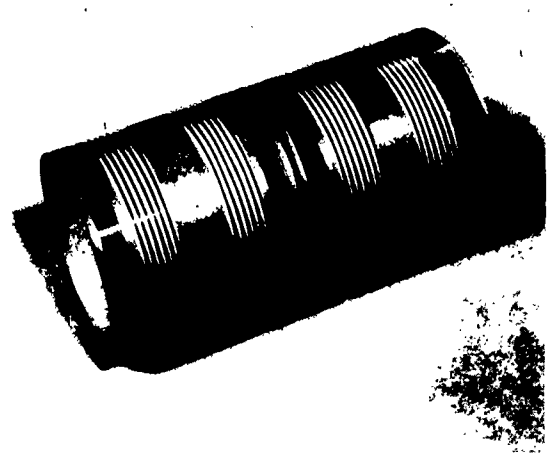

FIGURE 1.2: Coated Spiral Zoom-Lens

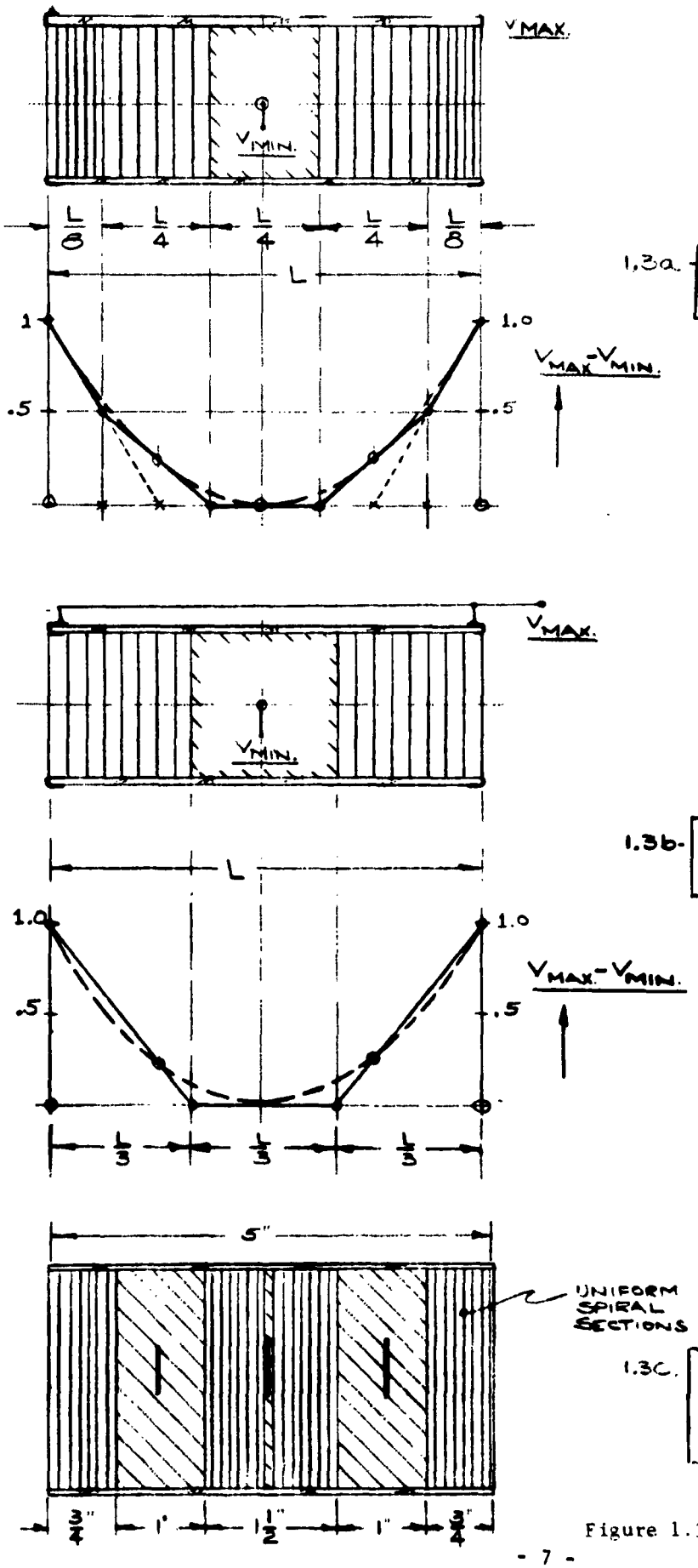

1.3a. TWO-STEP APPROXIMATION

1.3b. ONE-STEP APPROXIMATION

1.3c. ZOOM LENS SPIRAL WITH ONE-STEP APPROXIMATION

Figure 1.3- Spiral Lenses

1. THE SPIRAL-LENS COMPONENT (Continued)

Good and usable carbon spirals have been manufactured thus far by R. A. Wagner and J. Wilburt in this laboratory, using specially developed DAG-applicators of the pen-, or roller-, type. The glass surfaces to be coated are cleaned carefully by an HF-etch.

For mechanical and chemical protection, and for a more uniform field distribution, it is advantageous to coat the finished and baked spiral-lens with a thin film of material with very high resistivity. Such surface films also offer the important advantage of removing free charges between turns. Suitable materials for this purpose are powdered oxides of iron or chromium, or, better yet, Titanium oxide in a form recently developed on other Company-sponsored programs.

These surface films contribute to high-voltage stability by smoothing out high points of field strength and thus reducing corona discharge. Such film overlays do not interfere with the electron-optics of a spiral lens, provided they are sprayed on in thin layers.

The following notes present a few simple expressions for the design of resistive helixes and for the leakage introduced by coating these windings with films of high resistivity.

In Figure 1.4, a helix of N turns of resistive film is deposited on the inside of a glass cylinder with diameter D and length L. The surface then is coated to leak off free charges. The finished winding consists of Dag-stripes of width (s), separated by insulating gaps of width (g). The mark-to-space ratio then is $m = s/g$.

One-turn impedance

Figure 1.5 serves to derive an expression for the resistance of a single turn. In Figure 1.5-a, two adjacent turns are developed into a plane. This points up the number of series and parallel squares enclosed in one stripe (s) and one gap (g), respectively.

Figure 1.5-b shows the equivalent network for one single turn. It consists of a stripe-resistance r_s shunted by a leakage resistance r_ℓ. Both are given by equations (1.1a) and (1.1b):

$$r_s = \rho_s \cdot \frac{\pi D}{s} \qquad (1.1a)$$

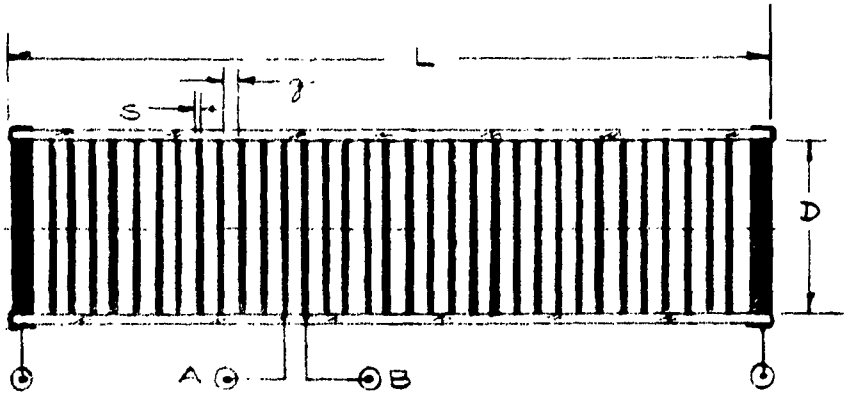

Fig. 1.4 - SPIRAL WINDING

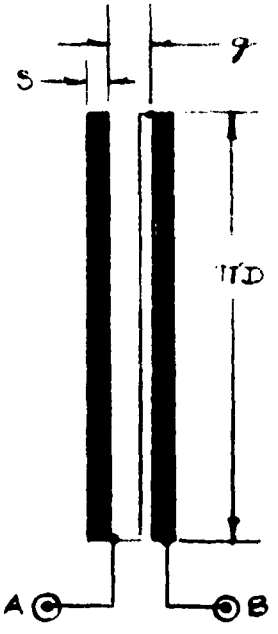

Fig. 1.5a
SINGLE-TURN NETWORK

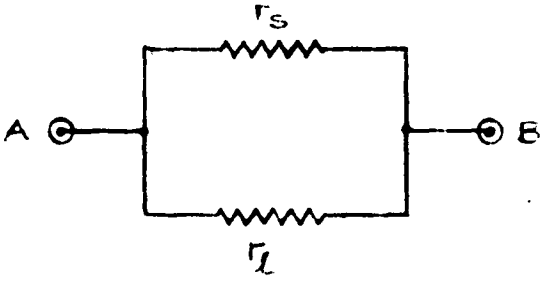

Fig. 1.5b
EQUIVALENT NETWORK

1. THE SPIRAL-LENS COMPONENT (Continued)

$$r_\ell = \rho_\ell : \frac{\pi D}{g} \qquad (1.1b)$$

Here, the factors ρ_s and ρ_ℓ are the respective thin-film resistivities of stripe and of insulation, in ohms per square. These thin-film resistivities (ρ) are related to the more commonly known volume resistivities (v) (ohm·cm) by the expression:

$$\rho = 100 \frac{v}{d} \qquad (1.2)$$

Here, (v) is the volume·resistivity in microhm·centimeters; and (d) is the film thickness in Angstrom-units ($1\text{Å} = 10^{-8}$ cm).

Equation 1.2 is only qualitatively correct. Numerically, it may be off by an order of magnitude, if handbook data are used for (v). This is especially true if loosely packed materials, such as graphite or Dag, deposited from a slurry, are considered. Typical data for turn impedances are given in Table I-A.

TABLE I-A

Typical Data for Spiral-Lenses

Material	length	dia.	spiral resistance	total turns	turn density	width of track gap		mark-to-space ratio	single-turn resistance:	
									stripe	gap
#	L	D	R_s	N	n	s	g	m	r_s	r_ℓ
Dag with neutral mix	4"	1"	100 meg	50	12	.060"	.030"	2	2. meg	>20 meg
Graphite	$\frac{5"}{8}$	1"	2 meg	$12\frac{1}{2}$	20	.025"	.025"	1	160 K	> 2 meg

Total Impedance

The end-to-end resistance of the entire spiral lens is a series-connection of N single-turn networks as shown in Figure 1.5-b. Accordingly, the terminal impedance can be found by multiplying equations (1.1a)

1. THE SPIRAL-LENS COMPONENT (Continued)

and (1.1b) by N, and keeping in mind that:

$$N \cdot (s + g) = L \quad \text{and } m = s/g \tag{1.3}$$

This yields the total spiral resistance R_s:

$$R_s = \rho_s \cdot \frac{\pi D}{L} \cdot N^2 \cdot \left(1 + \frac{1}{m}\right) \tag{1.4a}$$

as well as the shunt-resistance R_ℓ across the spiral terminals:

$$R_\ell = \frac{\rho_\ell}{\frac{\pi D}{L} \cdot (1 + m)}$$

From 1.4a, it is evident that, with a given material (ρ_s) and mark-to-space ratio (m), the spiral-resistance (R_s) increases with the square of the total turns (N).

On the other hand, equation (1.4b) shows that the shunt-resistance R_ℓ across the spiral is independent of the number of turns (N). For a given aspect ratio (D/L), R_ℓ depends only on the film resistivity ρ_ℓ and the mark-to-space ratio m = s/g. Shunt-leakage $\sim 1/R_\ell$ increases linearly with (m).

Optimum mark-to-space ratio

The influence of the mark-to-space ratio becomes apparent after dividing equation (1.4a) by equation (1.4b). This yields an expression for the "leakage-ratio" of a spiral lens:

$$\frac{R_s}{R_\ell} = \frac{\rho_s}{\rho_\ell} \cdot \left(\frac{\pi D}{L}\right)^2 \cdot N^2 \cdot \frac{(1 + m)^2}{m} \tag{1.5}$$

Since R_s is controlled by design, but R_ℓ is not, it is desirable to keep this leakage-ratio as small as possible, preferably below 10 per cent.

1. THE SPIRAL-LENS COMPONENT (Continued)

It is seen from equation (1.5) that the leakage-ratio goes through a minimum for m = 1; i.e., if the width of stripe and gap are equal.

Practical examples for spirals used in this project are given in Table I-B.

2. Spiral Coatings and Their Limitations

Progress has been made in the application of surface coatings, both in the cathode-lens section and in the spiral-lenses, as used here. This technique employs materials previously developed by Dr. Erwin Fischer-Colbrie of the Advanced Engineering Projects Operation of the Television Receiver Department on a Company-sponsored program.** The performance of coated spiral optics has been certified in the demountable, including field-flatteners and Zoom-lenses. These units were coated by thin films with a resistivity of 10^{10} ohms per square. The process of conduction in these materials is electronic, rather than ionic, so that long-time stability is no problem. With the above value of film resistivity, the overall resistance of the average spiral-lenses, as used in contract tubes, is affected very little (less than 5 per cent on the average). Several filmed spirals already have been tested in the demountable and were found to operate equally as well as uncoated units. This included the Zoom-lens tube. The coated-spiral lens used during the Zoom-lens development is shown in Figure 1.2. It has two spiral-lenses in tandem, each of them using the two-step approximation to a square law as described in Section 2.

Limitations of spiral coatings in phototubes

The usefulness of coated spirals has been certified from the electron-optical point-of-view. During the normal bakeout temperatures (450° max) encountered in the processing of cathode-ray tubes, coated spiral lenses may lose about 1/3 of their original resistance. This drop is not prohibitive for practical applications. Experience with TiO-coated spirals in tubes with S-9 photocathodes has been less favorable, as is more fully described in Section 7.

** It has been brought to our attention that similar work on Titanium-oxide films has been performed independently by Messrs. Willis, Winter, and Lauriente at the Westinghouse Electric Co. See: Transactions IX, Vacuum Symposium, 1962; pp 96-99.

TABLE I.B

Practical Data on Spirals

Material	volume resistivity	equivalent film thickness	film resistivity		trace width	1"-diam. resistance per turn	spiral resistance desired	turns total	spiral length for m = 1:	turn-density
	microhms x cm.	Angstroms	ohms/square		(s)	ohms	ohms	N	L=N·2s	n(tpi)
			stripe	gap						
Graphite	1000	100	1000	10^9	.025	125K	2.5 meg	20	1"	20
Dag with neutral mix	10^4	100	10^4	4.10^9	.050	625K	30 meg	50	5"	10

1. THE SPIRAL-LENS COMPONENT (Continued)

By contrast, coated spirals, temporarily exposed to cesium vapor, suffer a permanent loss of over 90 per cent of their resistance. This amounts practically to a short circuit across the spirals. It precludes the use of TiO coatings in photoelectric devices at the present state-of-the-art. As to future possibilities, reference is made to a special section on processing techniques contributed to this report by Mr. J. Roderick.

Fortunately, no such catastrophic resistance-drop was found, when uncoated Dag-spirals were used. All sealed-off samples of image tubes, described in the body of this report, used graphite-spirals on a clear-glass substrate. With these materials, the spiral-resistance-drop was not prohibitive; and no difficulties were encountered in removing cesium from its temporary adsorption on the spiral, or on the glass substrate, by conventional bakeout procedures.

C. High-Voltage Stability of Spirals

If spiral lenses are operated at high voltages, corona-discharge between turns is an effect to be reckoned with. The physical background for such discharge is field-emission from thin films. The onset of cold emission occurs at a field strength of approximately 10^7 volts/cm.

It is possible to give an estimate for high-voltage stability of electrostatic devices employing thin films. This is of some interest in connection with the present project, since spirals may be overloaded by high voltage before they are overheated by current.

The electrostatic field around a wedge has been analyzed by means of conformal mapping. In Figure 1.6, a sharp wedge of conducting material is shown as an equipotential Φ_o; and an electric field, intersecting the wedge orthogonally, is represented by a streamline ψ = const.

If both functions are considered as members of a family of confocal parabolas, there is a conformal transformation, which maps this family into a net of Cartesian coordinates. This transformation reads:

$$w = \sqrt{z} \qquad (1.6)$$

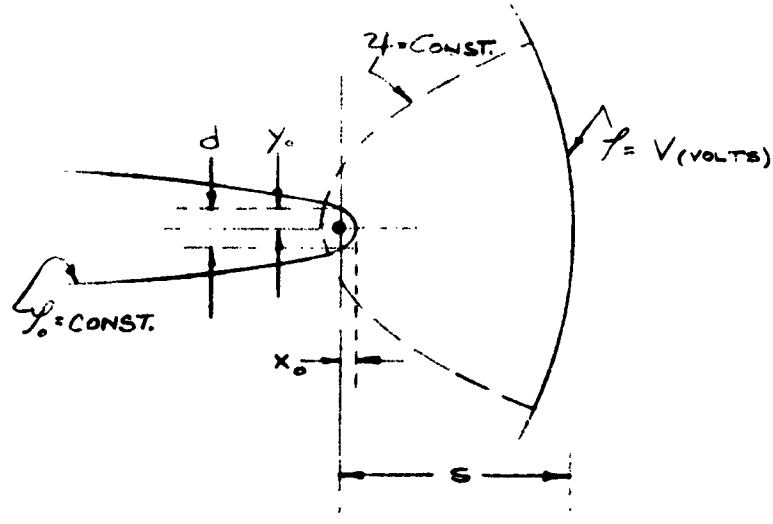

fig. 1.6: ELECTRIC FIELD AROUND A WEDGE

1. THE SPIRAL-LENS COMPONENT (Continued)

where $w = u + jv$, and $z = x + jy$. From (1.6), we get:

$$2\,(p\Phi)^2 = \sqrt{x^2 + y^2} + x \qquad (1.7a)$$

$$2\,(q\psi)^2 = \sqrt{x^2 + y^2} - x \qquad (1.7b)$$

Here, Φ = const and ψ = const are equipotentials and stream-functions; and p and q are constant factors, to be determined by the boundary conditions:

$$\begin{array}{lll} x = x_o & y = 0 & \Phi = \Phi_o \\ x = 0 & y = \frac{d}{2} & \Phi = \Phi_o \\ x = s & y = 0 & \Phi = V \end{array} \qquad (1.8)$$

This defines the wedge potential Φ_o and position x_o in terms of the sharpness (d) of the wedge:

$$\Phi_o = \frac{V}{2}\sqrt{\frac{d}{s}} \quad ; \quad x_o = \frac{d}{4} \qquad (1.9)$$

The highest field strength $\overline{E}_{max}$ occurs at the tip of the wedge: $y = 0$; $x = x_o$. This gradient follows by partial differentiation of Equation (1.7a):

$$\boxed{\overline{E}_{max} = \frac{\partial \Phi}{\partial x_{(x_o)}} = \frac{V}{s} \cdot \sqrt{\frac{s}{d}}}$$

Here, V/s is the field strength to be expected between parallel plates, or between large, smooth electrodes. The result (1.10) therefore may be expressed as follows:

> "If one of two parallel plates (distance "S") is folded back into a edge of thickness (d), the field-strength at that edge increases by the factor $\sqrt{s/d}$. In the process, the peak-gradient on the opposite plate decreases by 50 per cent."

In thin-film devices, this field-strength multiplier $\sqrt{s/d}$

1. THE SPIRAL-LENS COMPONENT (Continued)

can bridge almost three orders of magnitude! This can cause field-emission, followed by arcing. Practical data are given for spirals in Table I-C. Corona discharge may be assisted by free charges on the dielectric substrate. It may be retarded by coatings with high resistivity, even if such coatings protrude only very little (30,000 Å) beyond the borderline of the Dag-stripe. A high-resistance film (10^{10} ohms per square, or less), deposited on top of a finished spiral, greatly contributes to high-voltage stability, and to charge-removal, as well.

TABLE I-C

High-Voltage Limitations for Resistive Spirals

film-thickness (Angstrom)	turns per inch	field-strength multiplier $\sqrt{\frac{s}{d}}$	high-voltage limit between turns (volts)	average size of spiral lens unit	device application;
100	20	175	500	1" cylinders	e-s vidicons camera tubes
100	10	250	700	2-1/2" cylinders	image converters
100	5	350	1000	large 5" envelopes	UHR-displays (ultra-high resolution tubes)

2. FLOODGUN DEVELOPMENT

To simplify and to expedite the testing of various experimental gun structures for image tubes, it was decided to avoid the use of photoemissive cathodes during the early phases of the project and to use thermionic emission instead. To do so, a floodgun system, delivering a broad, parallel electron-flow at a controlled low voltage, was developed. This collimated electron flow, about 2-1/2 inches in diameter, was used to illuminate a perforated plane disc, serving as a simulated cathode. Figure 2.1 shows a photograph and a scale drawing of this K-plate, used in all early experimental work.

Since the floodgun cathode is at ground, the speed of flood electrons entering the test tube is defined by a bias voltage e_k applied between the K-plate and ground. This bias voltage e_k is henceforth referred to as the "injection voltage".

A. Design Objectives

In the design of the floodgun, the following objectives were sought:

1. The floodbeam should be well-collimated to land normally everywhere on the K-plate.
2. Current density should be as nearly uniform as possible.
3. Beam current should be under control by a grid.
4. All the above parameters should stay unaffected by variations of the cathode injection voltage.

B. Theory of Collimation

Figure 2.2-a shows the basic electron optics of the floodgun. A beam from a grounded CRT-cathode K* is first brought to a crossover C by a conventional triode gun G_1 - A_1 (A_1 = 300 volts). After the crossover, the beam enters into a large-diameter (3 inches) cylinder, which encloses a special kind of field. This field consists of two sections:

1. a section of field-free drift space: length (a)
2. a section with square-law potential on axis: length (b)

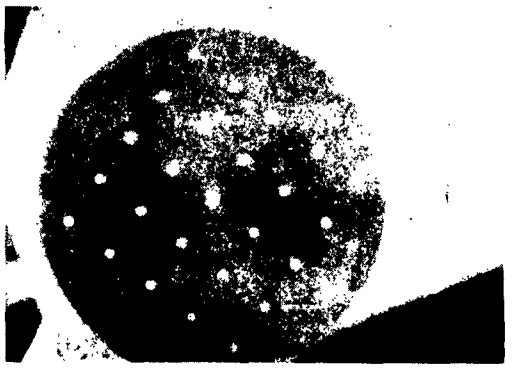

PHOTOGRAPH OF OBJECT MASK

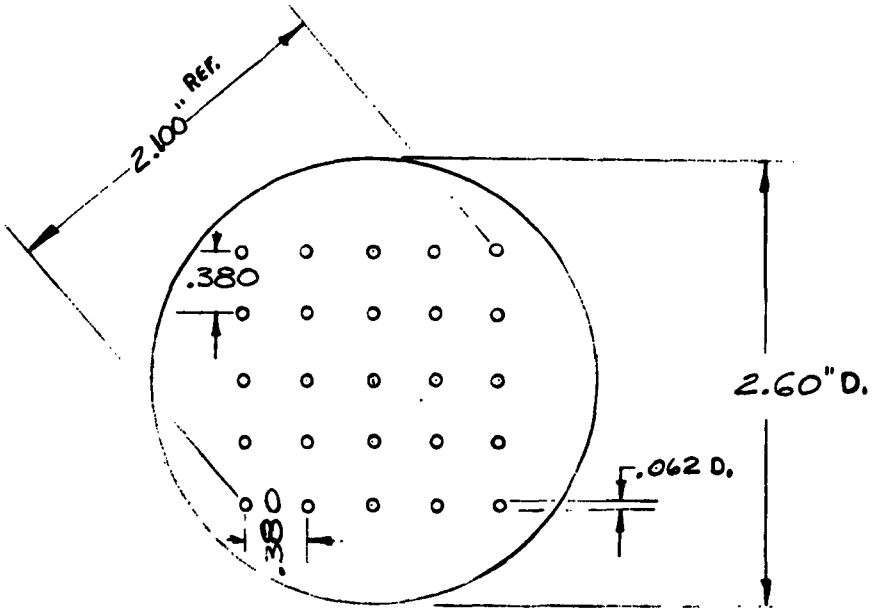

fig. 2.1 - PLANE OBJECT MASK

2. FLOODGUN DEVELOPMENT (Continued)

This type of field has been analyzed by Electron Trigonometry. The results indicate that a field as described can shape electron emission from a point source into a large-diameter parallel flow. To do so, it is necessary that certain numerical relations be observed between the ratio of distances, b:a, and of voltages, $p = V_2:V_1$. More specifically, the condition for collimation reads as follows:

$$\sqrt{2} \cdot \tanh^{-1} \frac{\sqrt{P-1}}{1+\sqrt{P}} = \tan^{-1} \frac{b}{a} \sqrt{\frac{2}{P-1}} \qquad (2.1)$$

A graph of this equation is shown in Figure 2.3. As an example, collimation will occur for a = b if the voltage stepup across the tube is slightly more than 3-to-1. Within limits, P can be used in practice to optimize collimation.

C. Spiral Optics

Figure 2.2-c shows the voltage distribution required on the wall of a cylindrical envelope in order to realize an axis potential, such as Figure 2.2-b. From the saddle point to the right, the dotted curve in 2.2-c is identical with the paraboloid shown in Figure 2.2-b, except for the subtraction of a fixed voltage drop of $\frac{c}{8}D^2$ (D = bulb diameter, and c = lens power). It thus becomes necessary to supply one separate boundary voltage W_o running somewhat below the first-anode potential (e.g., $A_1 = W_1$ = 300V, W_o = 150 volts).

The three solid tangents in Figure 2.2-c show a close approximation to the required non-linear distribution of wall potential. Three linear sections are used, including one conductive band ℓ_o at W_o volts ($W_o < A_1$), followed by two sections S_1S_2 of linear spiral winding with lengths of ℓ_1 and ℓ_2, respectively. The design of this two-stepped linear spiral has been explained in Section 1 in more detail. ℓ_2 measures 1/2 ℓ_1.

The collimation section in Figure 2.2-a is followed by deceleration in a linear spiral S_3. Both sections are separated by a plane mask M (30 holes per inch), connected to W_2 = 1,000 volts. Deceleration without focusing action requires a uniform spiral S_3 of constant pitch. This high resistance (20 megohms) spiral (S_3)

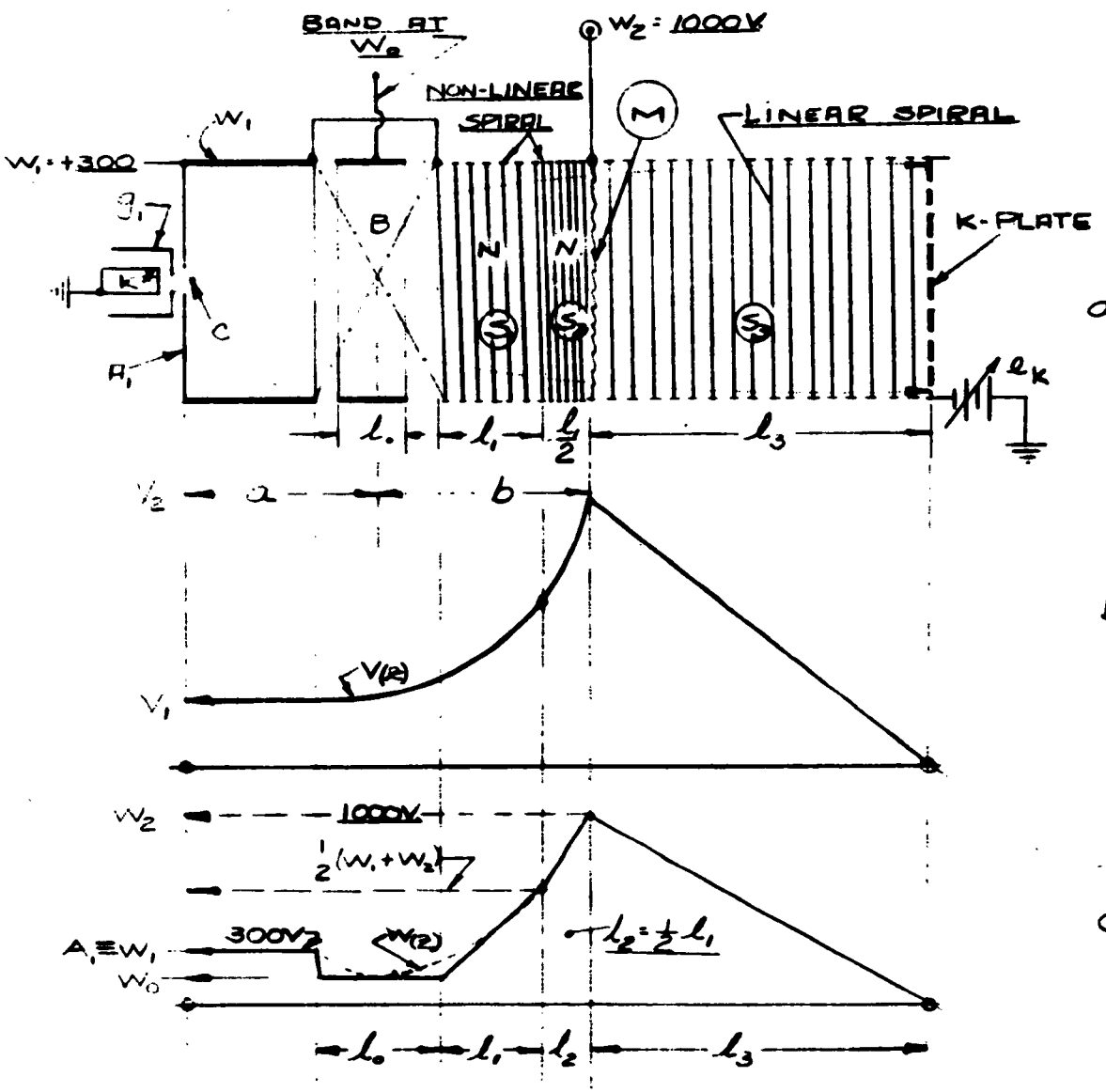

a. FLOOD-GUN CONFIGURATION

b. AXIS-POTENTIAL DISTRIBUTION

c. WALL-POTENTIAL DISTRIBUTION

fig. 2.2 - BASIC FLOODGUN DESIGN

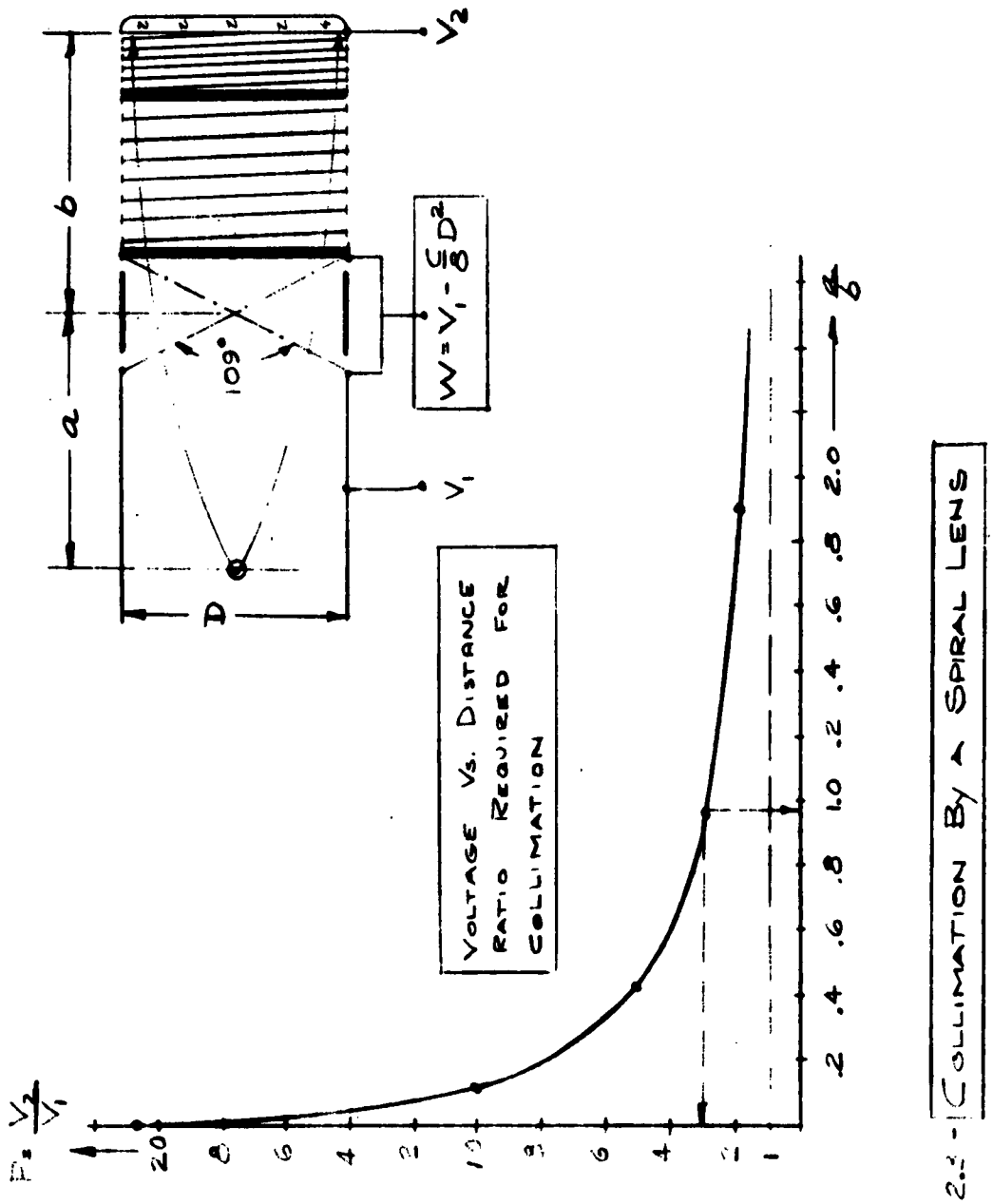

Fig. 2.2 - Collimation By A Spiral Lens

2. FLOODGUN DEVELOPMENT (Continued)

allows the endplate (K) to be connected to an arbitrary injection voltage e_k that can be varied without affecting collimation since $e_k < W_2$. The endplate (K) is actually the cathode of the image tube under test. It may be mechanically, though not electrically, disconnected from the floodgun.

D. Floodgun Performance

Figure 2.4 shows the floodgun assembly in its final form. This differs from Figure 2.2 mainly by the functional separation of intensity control, and of crossover formation. The former is done by the G_1-grid; and the latter, by a separate Einzel-lens F mounted at the end of the barrel A_2. In operation, F was grounded, resulting in a crossover of small size very near the exit plane of the Einzel lens.

Figure 2.5 shows a performance test of the floodgun. For these photographs, a 3-inch Willemite aluminized screen at 7KV was mounted 3 inches behind the K-plate.

For the photographs shown in Figure 2.5, floodgun voltages were set up as follows:

A_2 = 550 A_3 = 250 M = 1,500

Beam current was 1,700μA.

In the three conditions of Figure 2.5, the K-plate was biased as follows:

Conditions	Injection Voltage	Magnification Observed (Approx.)
A	e_k = + 500	1/2
B	e_k = + 80	2
C	e_k = + 25	4

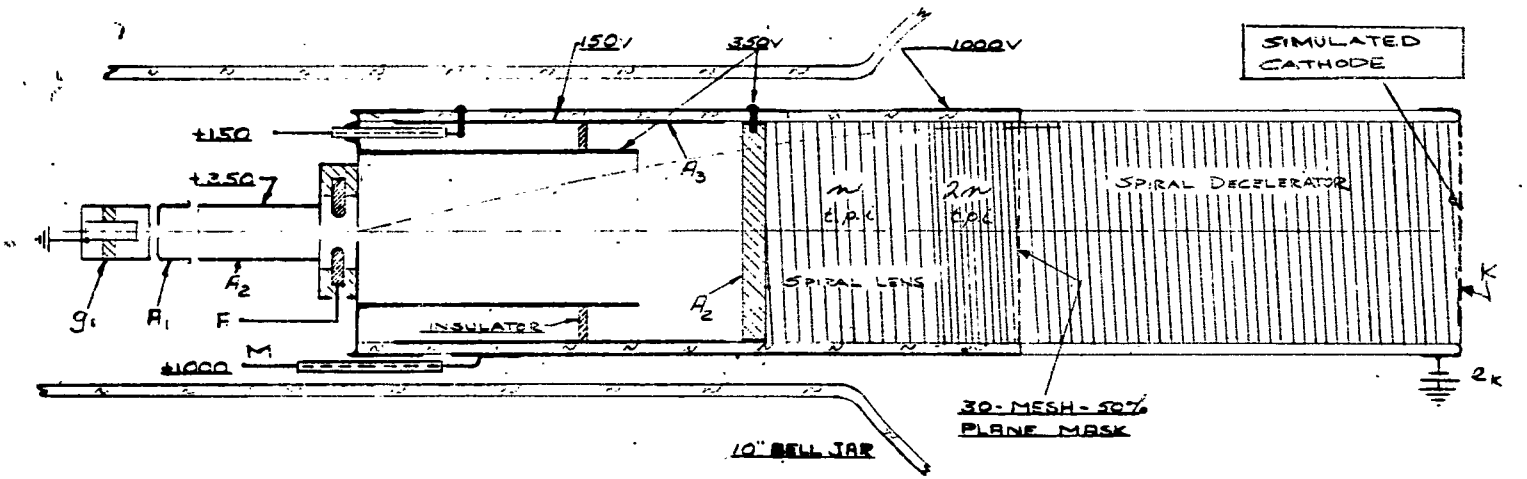

fig.2.4. FINAL FLOODGUN ASSEMBLY

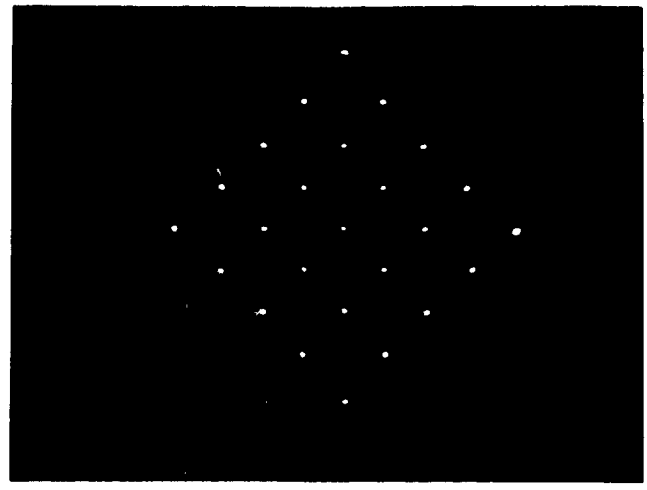

A. Object at +500V.

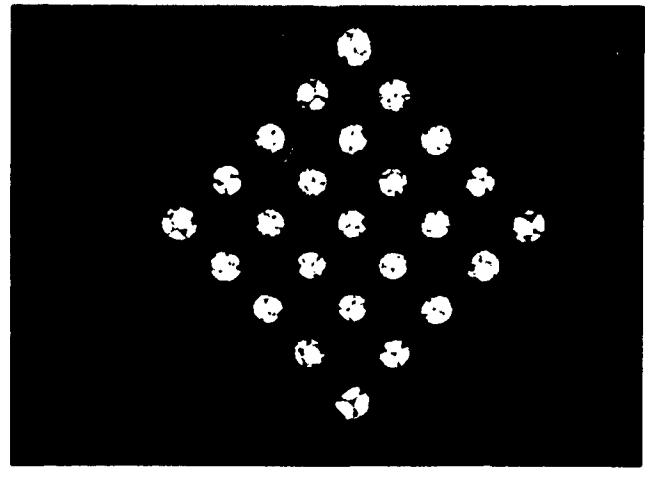

B. Object at +80V.

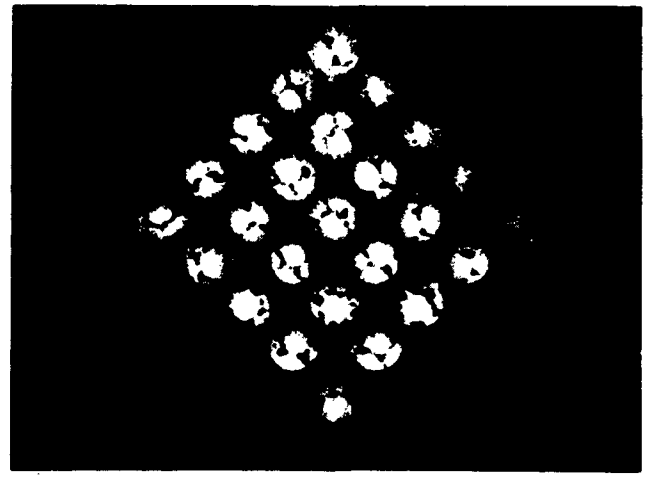

C. Object at +25V.

Figure 2.5

Floodgun Performance Test

2. FLOODGUN DEVELOPMENT (Continued)

It is observed that:

1. The center spacing between hole images is the same as that of the object plate (0.380").

2. This center spacing is conserved through all test conditions.

3. There is no variation of intensity across the entire image.

4. Magnification of the hole-images on the screen increases rapidly with decreasing injection voltage.

Points 1 and 2 imply that the beam is well-collimated upon arrival at the termination. This is supported further by the fact that the fine structure in each dot image is sharp. These black lines are actually shadows of the separator-mesh (M) located between collimator and the decelerator section. The throw for this shadow projection measured as much as 8 inches from object to screen.

E. Aperture Lens Effects

Point 4, the progressive enlargement of all holes, is due to the action of positive aperture lenses formed in the holes of the K-plate by the change of field on either side. The magnification as observed follows roughly the trend predicted by the Davisson-Chalbick formula. Gradients on both sides of the K-plate were -300 volts per inch before passage, and +2,000 volts per inch after passage.

In later applications, where the floodgun is used as a "light source" for image tubes, the outgoing gradient is generally much smaller. This reduces the power of the aperture lenses, and thus, the divergence of beams from individual apertures. As an extra precaution, the holes in the K-plate were covered up by fine metal gauze, offering the added advantage of presenting a high-resolution object.

3. FIELD-FLATTENER DEVELOPMENT

A. State-of-the-Art

The state-of-the-art shows that satisfactory images on a plane viewing screen are feasible as long as the cathode surface used is spherically convex.[14,15] Typical electrostatic image tubes are shown in outline on Figures 3.1-a and 3.1-b. These figures represent commercial designs of a diode- and a triode-type of image converter tube.[16] Typical data are given below:

TABLE III-A

Electrostatic Image Tube Data

Tube Type	Length (inch) (Electrical)	Useful Diameter		Cathode Radius R_k	Ratio R_k/D_k
		Cathode D_k (inch)	Screen D_s (inch)		
ITT Diode	1.9	0.65	0.5	1.13	1.75
ITT Triode	3.8	0.97	0.75	2.38	2.46
GE Triode	6.5	2.1	-	4.6	2.18

For comparison, dimensional information on our developmental tubes also is listed in Table III-A. These test tubes are scaled up approximately 2-to-1 over standard dimensions to facilitate gun assembly and testing in the laboratory. The flat cathode plate used has a maximum image diagonal of D_k = 2.1" (See Figure 2.1). Applying the 2:1 scale factor to the spherical cathodes of standard tubes yields a radius of curvature R = 4.6". This figure was set up tentatively as a design objective to be duplicated by our field-lens development. The resulting ratio $R_k:D_k$ = 2.18 is intermediate between corresponding figures for conventional diodes and triodes. It deviates in a direction anticipating that more, rather than less, than the conventional cathode would be required in developmental tubes. On this basis, our research effort proceeded toward two

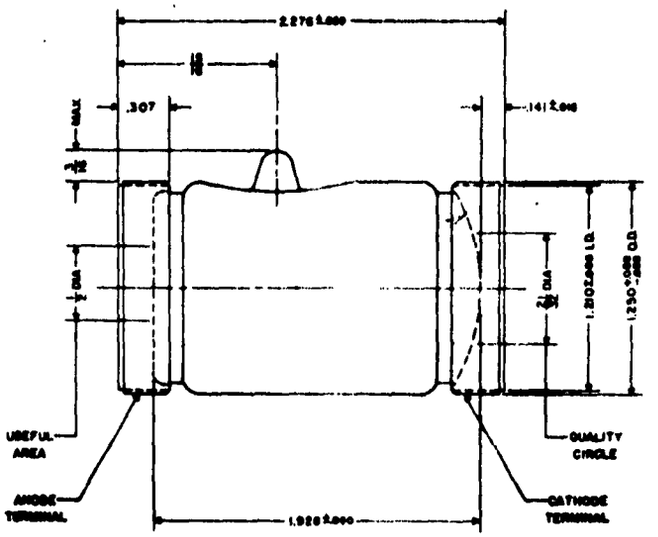

3.1a.

OUTLINE DRAWING

ITT - Type 7177/1C - 6

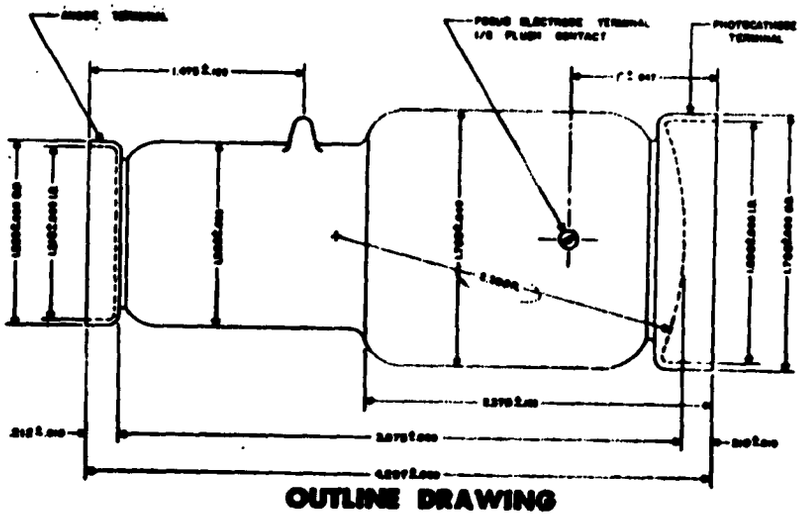

3.1b.

OUTLINE DRAWING

ITT - Type 6411/1C - 16-3

FIGURE 3.1

Commercial Electrostatic Image Tubes

3. FIELD-FLATTENER DEVELOPMENT (Continued)

objectives:

1. To develop an internal electronic field flattener so that plane cathodes can be used.

2. To accomplish image formation by means of spiral optics.

B. Ray-Tracing Analysis

As a first step toward objective 1, ray-tracing analyses were done on greatly simplified electrode structures. One typical example is given in Figure 3.2. Here we assumed a two-dimensional arrangement, consisting of a plane cathode K at ground potential facing a wire-anode of diameter (d) at distance (a). The equipotentials in this case are segments of cylinders as determined by equation 3.0:

$$\frac{V}{E} = \frac{\log \frac{1 - cz/a}{1 + cz/a}}{\log \frac{1 - c}{1 + c}} \quad ; \quad c = \frac{1}{\sqrt{1 - d/a}} \qquad (3.0)$$

The construction is explained by the sketch in the upper right of Figure 3.2.

Several of these equipotentials are shown in Figure 3.2. Two bundles of rays were traced through this field - one starting at the center of the cathode (A); the other starting at a radial distance 1 inch off center. In the process, the circle-path method was used.[17] The parabola method of ray tracing, however, also has been tried and has given similar results.[17,18]

As rays were traced through the field, tangents were projected backward from each equipotential reached to establish a virtual cathode, if one existed.

For the central ray from point A, this is known to be the case. All rays arriving at a plane-parallel anode spaced ℓ inches ahead of a plane cathode seem to originate from a virtual source placed ℓ inches behind it. (Point 23-0 in Figure 3.2.)

For marginal rays, this preliminary study indicated that a virtual image of an emission center on K is defined only for relatively close spacings, in terms of D, between anode mesh and

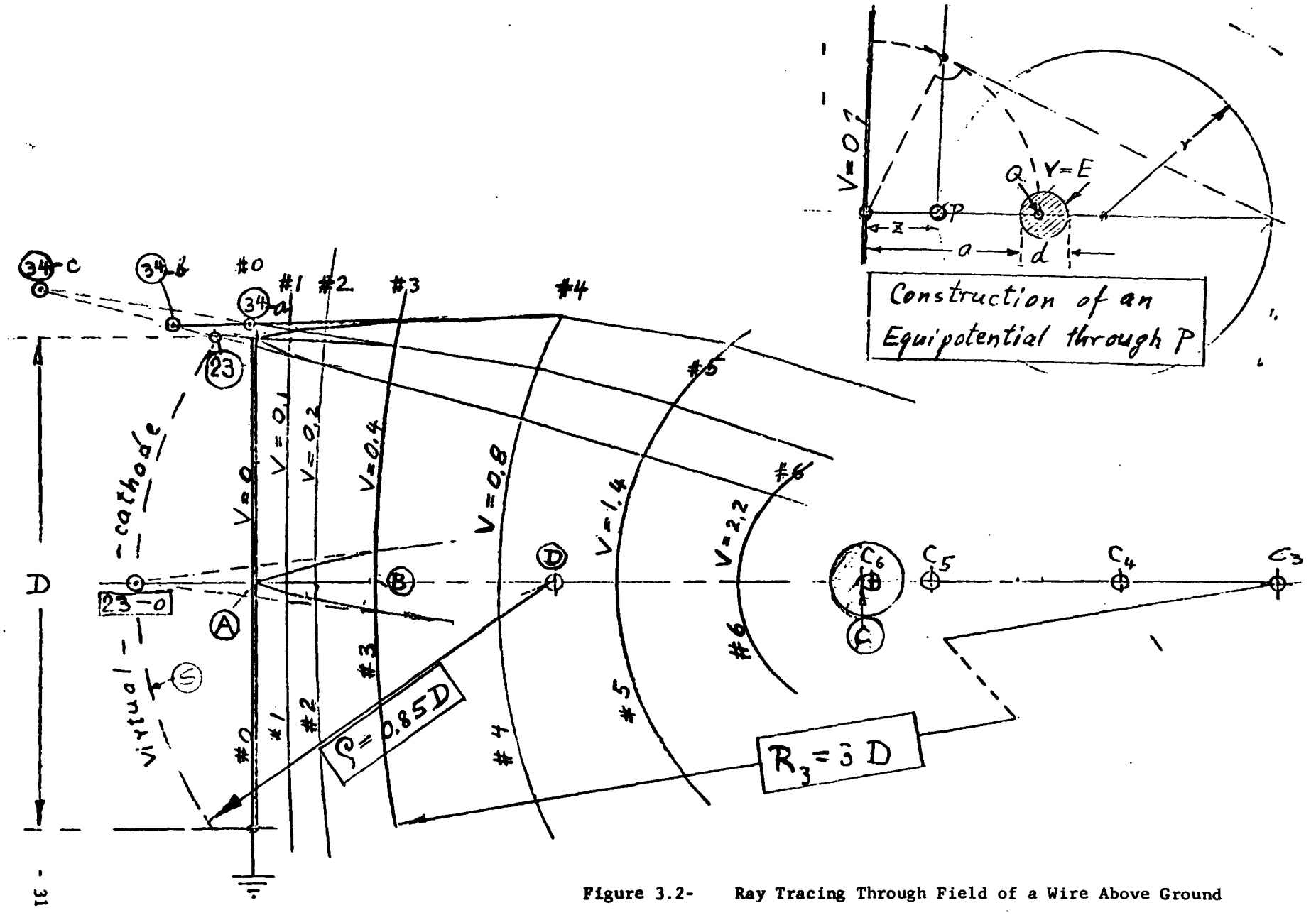

Figure 3.2- Ray Tracing Through Field of a Wire Above Ground

cathode. In Figure 3.2, the equipotential for V = 0.4E stands only 1/2 inch, or 1/4·D, away from cathode. This was found to be as far as one can go with anode spacing and still find a virtual cathode for marginal rays (point 23). For larger anode spacings, not one but several different image points were found between individual rays as shown at points 34-a, 34-b, and 34-c, respectively. This situation implies astigmatism and coma, and this fact has been borne out by observation (see Section 3C - Test Results).

Inspection of Figure 3.2 further shows that the connection of all virtual cathode images seems to lie on a cylindrical surface (S) behind the plane cathode. This surface is convex to the outside. More specifically, an internal anode mesh with R = 3D, or six (6) inches, radius of curvature, spaced 1/2 inch away from a 2-inch cathode plane, appears to simulate a convex cathode surface with 1.7-inch radius. This seemed promising.

It was realized that this simple analysis is unable to yield quantitative information; however, the general trend as indicated here seemed to be in the right direction. It therefore was decided to follow up by an experimental test.

C. Curved Anode Structure

Figure 3.3 shows the first experiment. A plane cathode (K), built as in Figure 1.1, was mounted in electrical and mechanical contact with the output spiral of the floodgun. This K-plate was followed by a 30-mesh anode A_1 facing the plane cathode K with a convex spherical surface (R = 3.75") at close range (1/4"). A focusing field was established within the volume enclosed by the spherical mesh A_1 on one side, and a plane separator mesh (S) on the other. The 2-1/2" x 2-1/2" glass cylinder between both meshes was coated in a manner resulting in a non-accelerating spiral lens (see Section 1). The mid-band (B) of this unit was brought out for focusing. The relative length and pitch of all spiral sections were designed as in Figure 1.1-c. With both mesh terminations at +1000 volts, and with the centerband near zero, a hyperbolic field could be established to a good approximation within the volume enclosed by the spiral lens. No constricting apertures were used in any of the experiments.

The separator (S) was a wire-woven mesh of low resolution (10 mesh per inch) and high transmission (80 per cent). This separator then was followed by a voltage-linear accelerating field. This was generated by a spiral (T) with constant pitch extending from S to the metallized screen U. This 3-inch spiral section acted as a non-focusing accelerator from 1000 volts in the lens to 10 KV at the screen. For the system as shown in Figure 3.3,

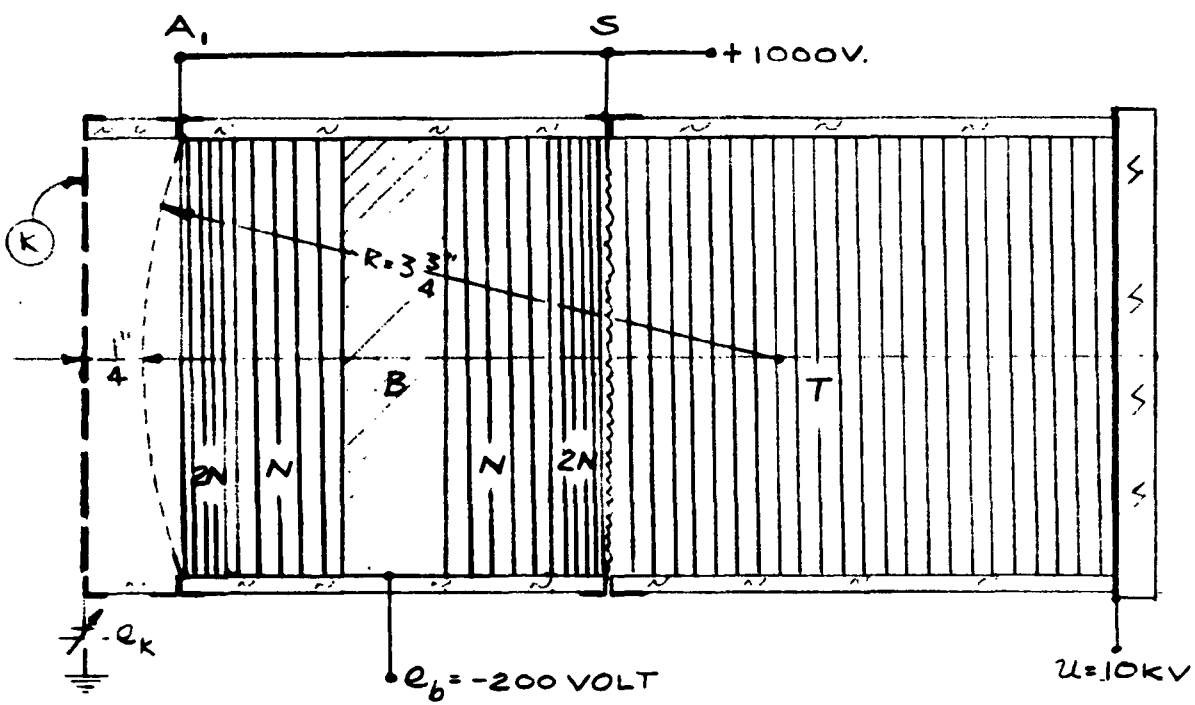

fig.3.3 - Curved-Anode-Type Field Lens

3. FIELD-FLATTENER DEVELOPMENT (Continued)

Electron Trigonometry[19] predicted an overall magnification of 1.27-to-1. Values found in practice ranged from 1.17 to 1.30.

Test Results

Typical images obtained with this device are shown in Figure 3.4-a. This image shows several major defects, including the following:

1. curvature of field
2. coma
3. limited field of view
4. pincushion distortion

To illustrate point 1, Table III-B presents a typical set of voltages required at the lens band B to bring various image areas into focus.

TABLE III-B

Focus-Variation Due to Curvature-of-Field

Image Area Brought into Focus	Lens Voltage e_b required
Center	-220
First Zone	-160
Second Zone	-70

This trend is plotted in Figure 3.5-a in per cent of first-anode voltage. The spread of 2-to-1 for these focus voltages indicates that a large amount of the field curvature has escaped correction by the field lens. The effectiveness of the latter, if any, seemed to be quite limited!

In order to determine whether the curved anode mesh A_1 had any effect at all, a second test was done with the same tube. This time, the field mesh A_1 was inverted so that its first surface

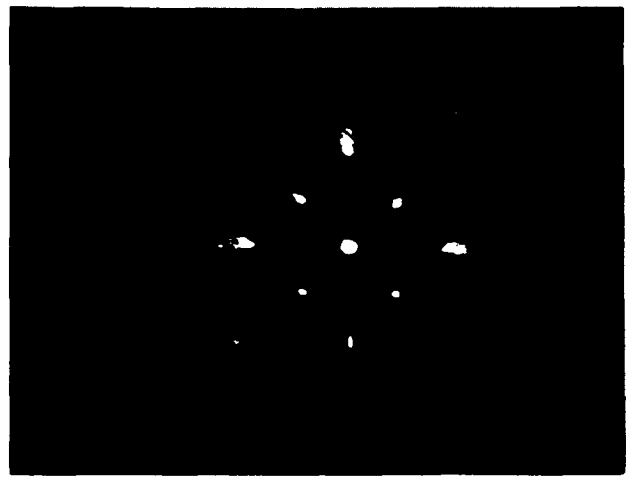

A. Field Mesh Convex

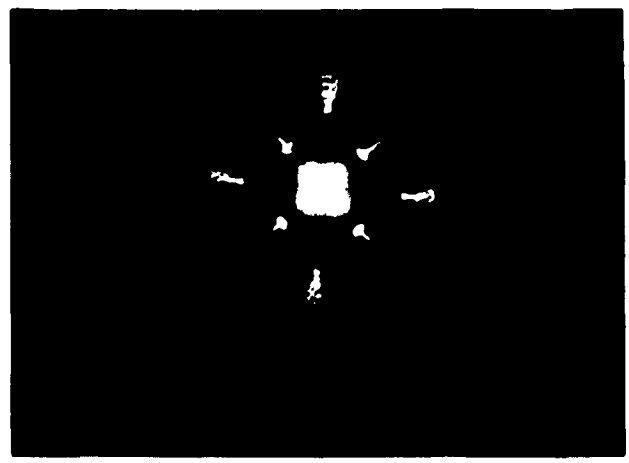

B. Field Mesh Concave

Figure 3.4

Results with the Curved Anode

was concave, rather than convex as seen in the direction of flow. The results are shown in the photograph in Figure 3.4-b. These results indicate that the aberrations have gone from bad to worse!

The same trend also is evidenced by Figure 3.5-b, which shows the spread of focus voltages observed with the field-mesh concave. This time the percentage focus variation varies as 4-to-1 from center to edge. This spread is twice as large as that observed before when the mesh anode was in the convex position.

The above test results may be summarized as follows:

> "There is experimental evidence for some limited effectiveness of a thin, internal field-lens, consisting of a spherical convex mesh in close proximity to a plane cathode. This action, however, is too weak to be useful as a field flattener in practical devices."

For this reason, and because of many other aberrations (some of them severe), a better approach to the problem was sought.

D. A Plano-Convex-Type Field Lens

1. Two Plane Parallel Meshes

A working theory, which has led to improved device design, has been derived from the electron optics between plane electrodes. This is illustrated in Figure 3.6-a, which shows an aperture A in grounded plane #1, assumed to pass emission from a grounded source toward a plane anode #2 (Voltage +E, distance s). Due to the parabolic nature of the trajectories, all electrons from (A) seem to originate from a common point (C) located at a distance (2s) behind the anode #2. (C) is therefore the electron image of (A).

Figure 3.6-b shows the same source illuminating an aperture (B) in a plane #3. This plane is at a distance (a) from anode #2, and it is connected to a positive voltage E/P. It then can be shown that this second aperture (B) will share with the first (A) the same electron image (C), provided that the voltage ratio P is adjusted to meet the condition:

$$\frac{b}{a} = \frac{\sqrt{P} - 1}{\sqrt{P} + 1} = g_{(P)} \qquad (3.1)$$

a. CONVEX ANODE MESH

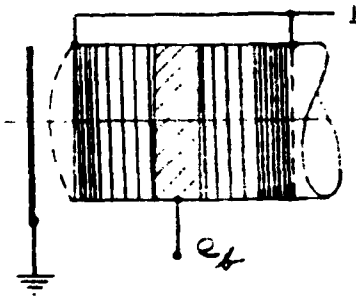

b. CONCAVE ANODE MESH

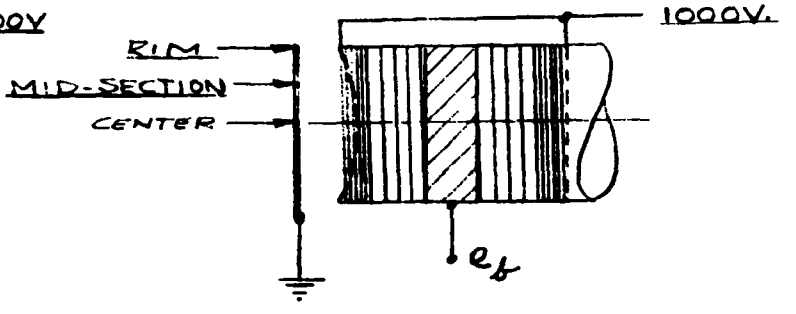

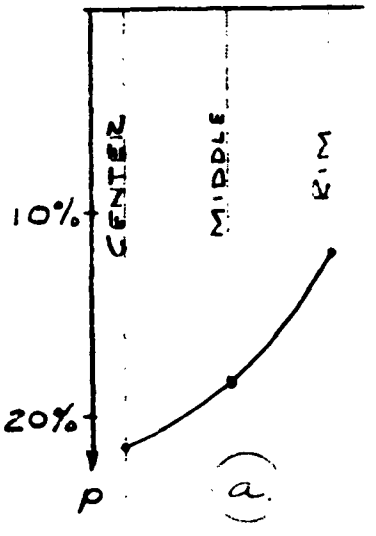

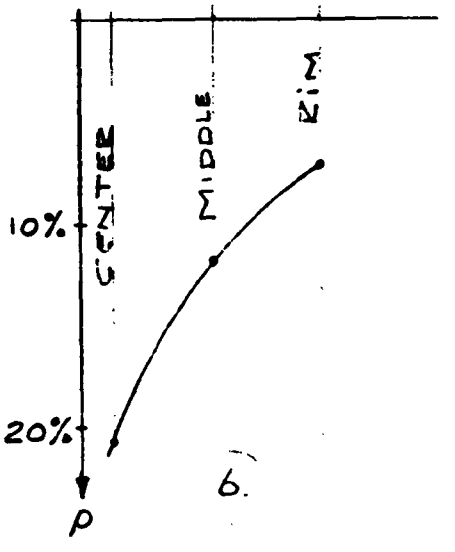

ρ = PERCENT FOCUS VOLTAGE CHANGE

$$\rho = \frac{e_c - e_r}{e_m} \cdot 100 \left[\%\right]$$

NOTE - e_c e_m e_r ARE VOLTAGES FOR PARTIAL AREA FOCUS

fig. 3.5 - CONVEX Vs. CONCAVE ANODE

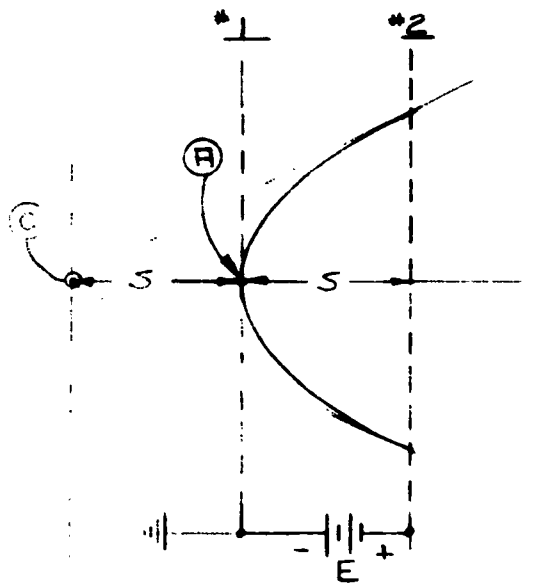

a. Grounded-Mesh To Anode

$$\frac{b}{a} = \frac{\sqrt{P} - 1}{\sqrt{P} + 1}$$

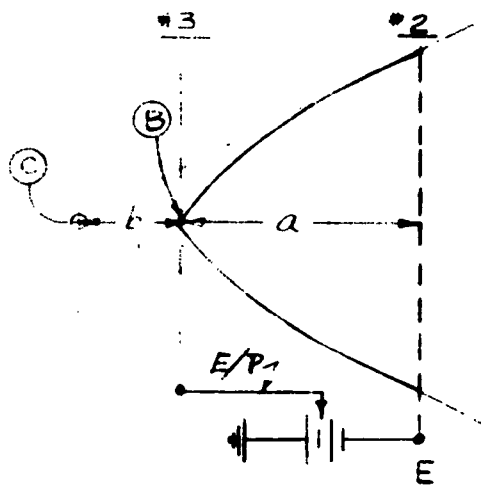

b. Biased Mesh To Anode

fig. 3.6- Equivalent Optical Planes

3. FIELD-FLATTENER DEVELOPMENT (Continued)

This optical correlation is valid for acceleration and deceleration alike. In essence, equation (3.1) implies that a source at one injection voltage and position may be replaced by a second source at some other injection voltage and position without this fact being noticed by an optical system focused at the virtual image of the first source.

2. One Plane and One Convex Mesh

This trading of position for voltage can be put to use in designing an electron-optical field-flattener or "aplanatic lens". This is illustrated best in connection with the specific problem at hand.

Figure 3.7-a shows a conventional type of image converter diode with spherical geometry.[20,21] This image tube includes a domed cathode K* with curvature 1/R and a point anode A at a high voltage U (10 KV).

An attempt is being made to replace this structure by the one shown in Figure 3.7-b. This structure uses a triode-type of field lens comprising a plane cathode K plus two meshes, M_1 and M_2. M_1 is a flat, high-resolution mesh mounted close to cathode K and connected to a variable injection voltage $e_k = E/P$. The mask M_2 is a highly curved, low-resolution mesh connected to an intermediate voltage $E < U$, ($E = 1000$ volts, $U = 10{,}000$ volts). In figure 3.7-b, the point anode A has been redrawn from Figure 3.7-a. The accelerating field between M_2 and A then represents the main focusing field, following the field flattener section between M_1 and M_2. In our developmental tubes, this focusing lens M_2-A has been replaced by a non-accelerating spiral lens (See Section 4).

In Figure 3.7-b, the equivalent curved cathode K* has been redrawn from Figure 3.7-a (dotted line). This is done only to facilitate the derivations that follow. In the finished device, there is no electrode in the space between M_1 and M_2.

3. Dimensional Analysis

An attempt has been made to get some first-order information about the shape of the second mesh M_2. Preliminary considerations show that this will have to be a surface of hyper-convex shape as shown in Figure 3.7-b. This follows from the fact that the image throw, i.e., the projected radial between K* and M_1, increases from a value a_o on axis to larger values s_o off axis. Equation 3.1

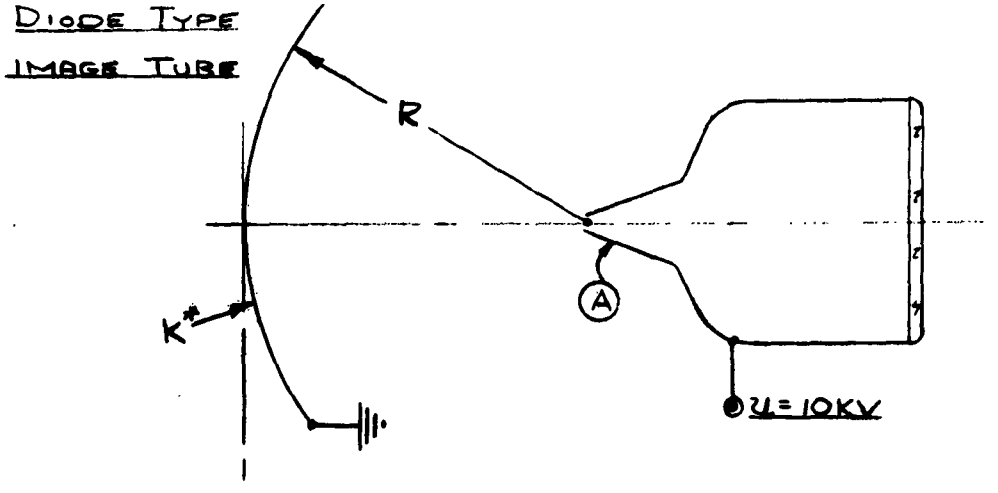

3.7 - a

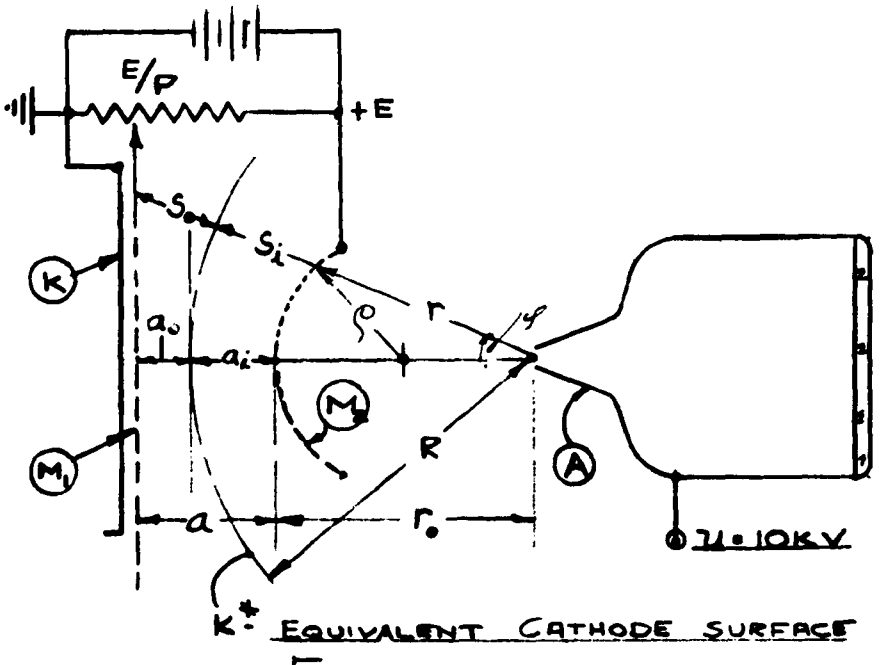

3.7 - b

[SHOWN ONLY FOR PURPOSE OF DERIVATIONS]

fig. 3.7 PLANO-CONVEX CATHODE LENS AND EQUIVALENT CATHODE

defines only the ratio, but not the absolute value, of image and object distances on either side of K*. Thus, it is feasible to increase a_o to s_o, by proportionally increasing a_i to s_i; i.e., by bending the field mesh M_2 even more than the equivalent cathode surface K* to be simulated.

The following equations may be written for Figure 3.7-b:

$$\frac{a_o}{a_i} = \frac{s'_o}{s_i} = g_p = \frac{\sqrt{P} - 1}{\sqrt{P} + 1} \tag{3.2}$$

$$\frac{R + a}{\cos \Phi} - R = s_o \tag{3.3}$$

$$R - r = s_i \tag{3.4}$$

Dividing equation (3.3) by equation (3.4) and using equation (3.2) yields:

$$r = R \left[1 + \frac{1}{g} \left(1 - \frac{1}{\cos \Phi} \right) \right] - \frac{a}{1 + g} \tag{3.5}$$

where $a = a_o + a_i$ is the physical separation between field mesh M_2 and cathode mesh M_1. Setting $\Phi = 0$ gives the vector r_o to apex:

$$r_o = R - \frac{a}{1 + g_{(p)}} \tag{3.6}$$

Subtracting equation (3.5) from equation (3.6) gives the desired expression for the profile of the field mesh:

$$r_o - r = \frac{R}{g_{(p)}} \left[\sec \Phi - 1 \right] \tag{3.7}$$

3. FIELD-FLATTENER DEVELOPMENT (Continued)

This is the equation of a "conchoid", which is also called a "shell curve".[22]

To find the radius ρ of the approximate sphere at vertex, Figure 3.7-b is read:

$$2\rho\,(r_o - r) = (r \cdot \sin\Phi)^2$$

whence ρ can be found by the transition:

$$\rho = \frac{r_o^2}{2} \cdot \lim_{\Phi = 0} \frac{\sin^2\Phi}{r - r_o} = \frac{g}{R} \cdot r_o^2 \qquad (3.8)$$

The result is:

$$\frac{\rho}{R} = g_{(p)} \left[1 - \frac{a/R}{1 + g_p} \right]^2 \qquad (3.9)$$

This result yields the curvature $1/\rho$ of the field mesh M_2 required to simulate a spherical cathode K* with specified curvature 1/R.

4. Equivalent Spherical Cathode

Often it is more important to find 1/R once the doming $1/\rho$ of the field mesh M_2 and its distance (a) off cathode are known. Solving (3.9) for R yields this information in the form of equation (3.10):

$$\frac{R}{\rho} = \frac{1 + \sqrt{1 + \frac{4 \cdot g}{1 + g} \frac{a}{\rho}}}{2 \cdot g_{(p)}} + \frac{a/\rho}{1 + g_{(p)}} \qquad (3.10)$$

where:

$$g = \frac{\sqrt{P} - 1}{\sqrt{P} + 1}$$

This function is plotted in Figure 3.8 for various spacings a/ρ between the two meshes.

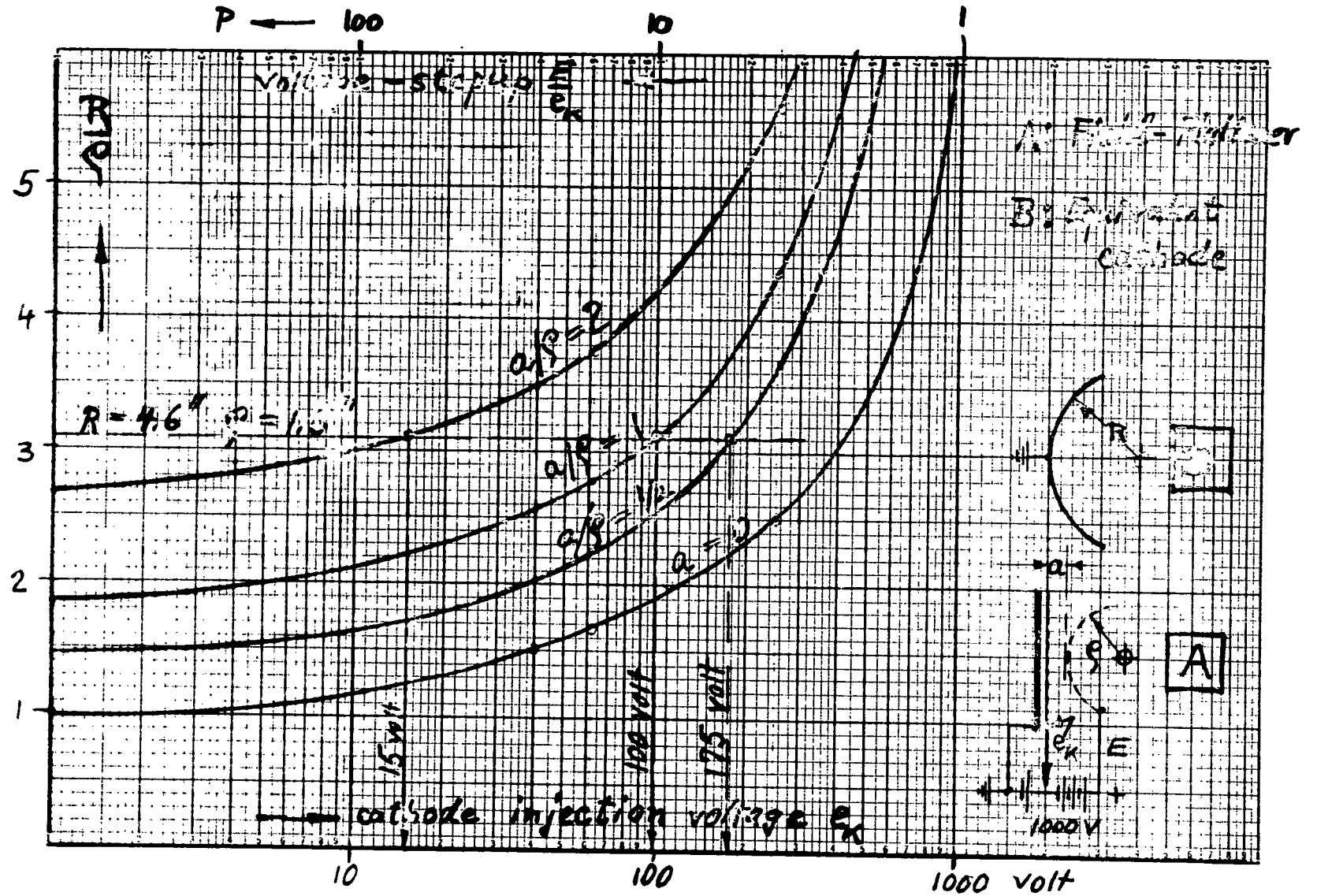

FIGURE 3.8- Aplanatic Lens

3. FIELD-FLATTENER DEVELOPMENT (Continued)

The general trend of these curves is as expected. Specifically, we find that:

1. $R \longrightarrow \rho$ as $P \longrightarrow \infty$, $e_k = 0$

2. $R \longrightarrow \infty$ for $P = 1$, $e_k = E$

3. R/ρ increases with a/ρ.

The horizontal line shown through $R/\rho = 3.1$ corresponds to data encountered in the experiments; namely, $R = 4.6"$ and $\rho = 1.5"$ (see Table III-A).

Figure 3.8 then indicates that this condition will occur at a cathode injection voltage $e_k = 175$ volts, if the system length is $a/\rho = 0.5$, $a = 0.75"$. Smaller injection voltages will have either a stronger effect in a system of given length, or else they will have the same effect in a longer system. For example, in a system with $a/\rho = 2$, or $a = 3$, inches length, it will require only 15 volts, rather than 175 volts, to correct for the same curvature of field.**

Despite the simplifying assumptions used at the start, this approximate analysis has come closer than was expected in describing actual device performance of this aplanatic lens.

5. Experimental Test of Field Lens

To check on the above theory of the plano-convex field-lens, a number of test tubes were built and tried in the demountable. Generally, the results were much better than those obtained with the earlier curved-anode structure.

Figure 3.9 shows a typical field-flattener section developed on the basis of concepts presented above. It

**It should, of course, be realized that the first-mesh voltage is dictated, in practice, by considerations other than ease of stop-motion operation. In actual image converters, the reduction of pencil spread at cathode is an overriding condition. This favors high, rather than low, M_1 voltages (see Section 4).

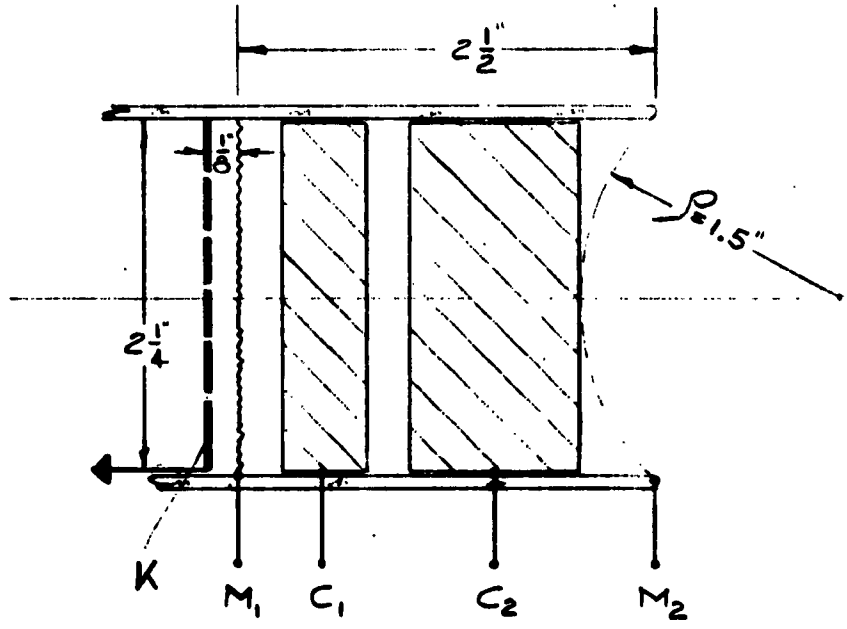

fig 3.9- PLANO-CONVEX FIELD LENS

3. FIELD-FLATTENER DEVELOPMENT (Continued)

is terminated at the input end by a plane cathode K, followed closely (1/8") by a planar mesh M_1 that serves as the first anode. At the output end, the field-flattener is terminated by a hyperconvex mesh M_2 at 500 to 1,000 volts.

Two rings, C_1 and C_2, were used originally to study the effects of various potential distributions between M_1 and M_2. In later stages of this development, it has been possible to combine both rings, C_1C_2, into one cylinder C_{12}, thus reducing to one the number of voltages required for adjustment. This field flattener was first tried in an image tube shown in Figure 3.10. At first, this tube did not have a cathode mesh M_1, but used instead a variable injection voltage e_k at K directly. Two 1/4-inch rings, R_1 and R_2, were brought out for external control of the wall potential between the K-plate and the field mesh M, which was heavily domed (ρ = 1.5 inches; a/ρ = 1/2). This mask covered the input end of a non-accelerating spiral lens. The lens output was covered by a flat mesh separator (S), which was used in early tests to shield the lens volume from the accelerator volume. In later tests, this separator mesh was removed. No beam-confining apertures were used within this tube assembly.

A typical image obtained with this device is shown in Figure 3.11. While the earlier pictures showed only 9 of the 25 dots in the K-plate, the new optics displays 21 of them with fairly good geometry.

The focus uniformity in Figure 3.11 was not perfect; however, it was found that this could be improved as the cathode injection voltage e_k was raised from zero. To show this graphically, the three voltages e_c, e_m, and e_r required at the spiral lens to focus on center, mid-range, and rim of K were measured for any one setting of e_k. This yielded the percentage focus variation:

$$p = \frac{e_c - e_r}{e_m} \cdot 100\%$$

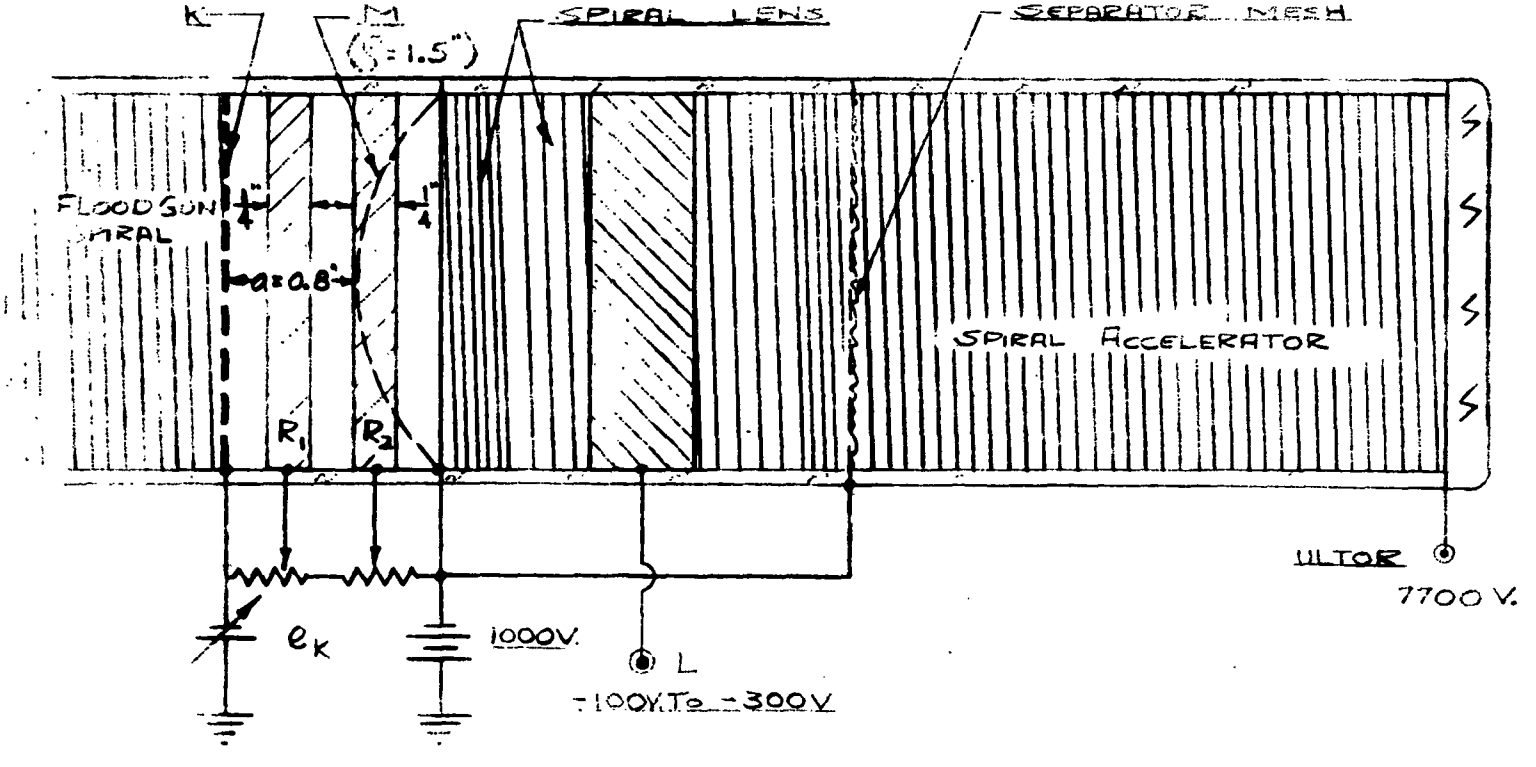

Fig. 3.10 — SPIRAL-LENS TUBE WITH APLANATIC CORRECTOR LENS

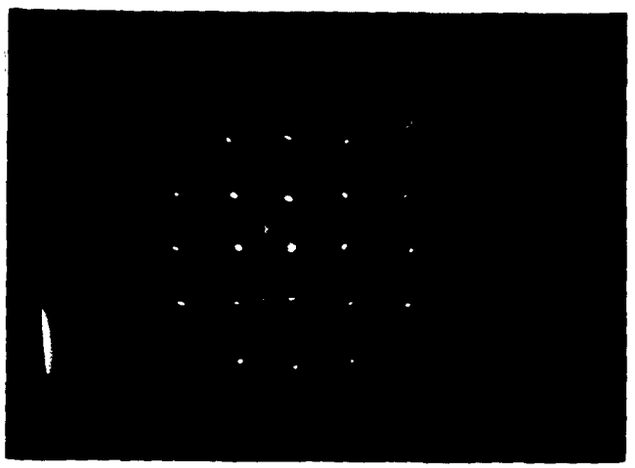

Figure 3.11

Image Obtained with Tube of Figure 3.10

3. FIELD-FLATTENER DEVELOPMENT (Continued)

This is plotted in Figure 3.12 as a function of the cathode injection voltage e_k. It is seen that the need to refocus decreases sharply as e_k is raised from zero to +80 volts. Beyond that value, focus aberrations seem to reappear. This trend is in general agreement with the analysis of the plano-convex field flattener as developed above.

6. Field Lens with Plane Cathode Mesh

The next step was directed toward tube operation with the cathode at ground. To do so and still have high injection velocity required the addition of a separate plane, mesh anode near cathode (Figure 3.9). To accomplish this, the system of Figure 3.10 was modified by the addition of a fine mesh M_1 (250 m) stretched out flat and 1/8 inch away from the simulated cathode K. It was now feasible for the first time to operate the image tube with cathode on ground while the field flattener could be adjusted separately. This method provided a more realistic simulation of conditions found in practice.

Figure 3.13 shows three types of pictures obtained under conditions as follows:

Photo No.	Cathode Plate	First Anode Mesh M_1	Spiral Lens Focus Voltage
A	Grounded	+250	-110
B	Grounded	+250	-30
C	Grounded	+45	0

In the first two conditions, with M_1 at +250 volts, defocusing caused by curvature of field is quite pronounced. In the terms used before, a focus readjustment of 57 per cent was required to cope with this aberration. In condition C, with M_1 lowered to +45 volts, focus is much more uniform over the entire cathode area. The existence of an optimum injection voltage is in general agreement with the theory of the device, notably Figure 3.8.

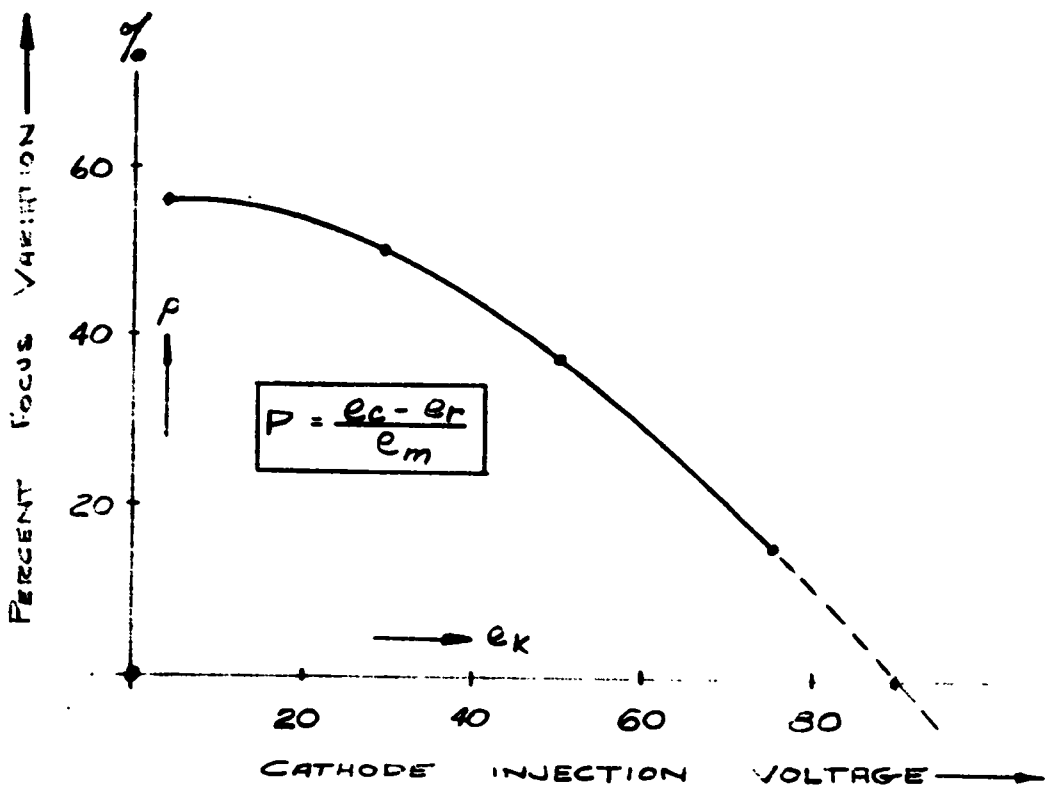

fig.3.12- FOCUS-VOLTAGE VARIATION AS A FUNCTION OF INJECTION VOLTAGE

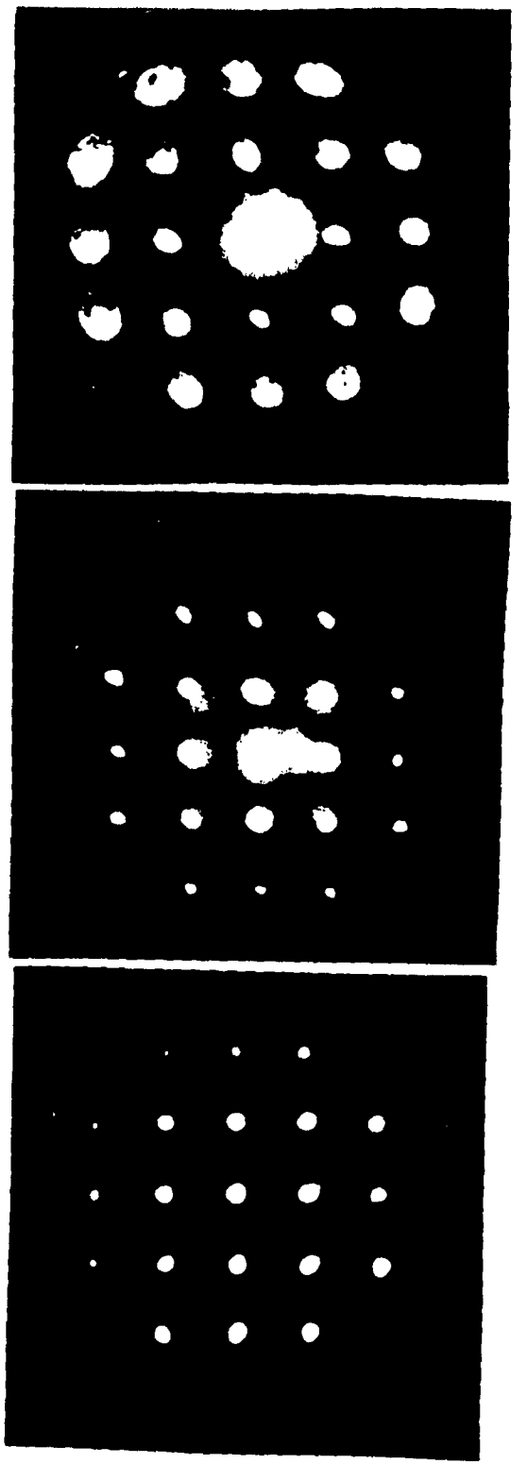

a.

b.

c.

Figure 3.13- Correction for Curvature of **Field**

3. FIELD-FLATTENER DEVELOPMENT (Continued)

7. An Orthoscopic Lens Doublet

Toward the end of the field-flattener development, a separate experiment was performed in order to justify the use of a domed, rather than a plane, mesh termination. Figure 3.14 shows the type of gun used (a) and its approximate axial voltage distribution (b). This cathode lens system is almost identical with the one described before (see Figure 3.9), except for the fact that the hyperconvex field mesh at M_2 has been placed by a plane mesh in the same location.

The test consisted of searching for a condition of optimum flatness of field, by adjusting the voltages on terminals C_{12} and (F) and thus balancing the relative powers of cathode-lens and spiral-lens sections. In the process, voltages at the lens-terminations M_1, M_2 and U were held constant.

Typical results are shown in the photographs of Figure 3.15. The three conditions shown there used bias voltages as listed in Table III-C below.

TABLE III-C

Voltages Used in Photograph 3.15

Condition Marked As	M_1	$C_1 = C_2$	M_2	F	U	Center Focus	Edge Focus	Overall Magnif.
a)	500	220	1000	0	5000	Out	In	-
b)	500	250	1000	-170	5000	In	In	0.42
c)	500	280	1000	-200	5000	In	Out	-

The photographs show one condition (b) for which the focused area is a maximum, inferring a minimum curvature of field. At the same time, other aberrations seem to have improved, too. These include: distortion, coma, and astigmatism, in that order.

Distortion can be judged best by viewing the photos from a glancing angle. It then will be observed that in

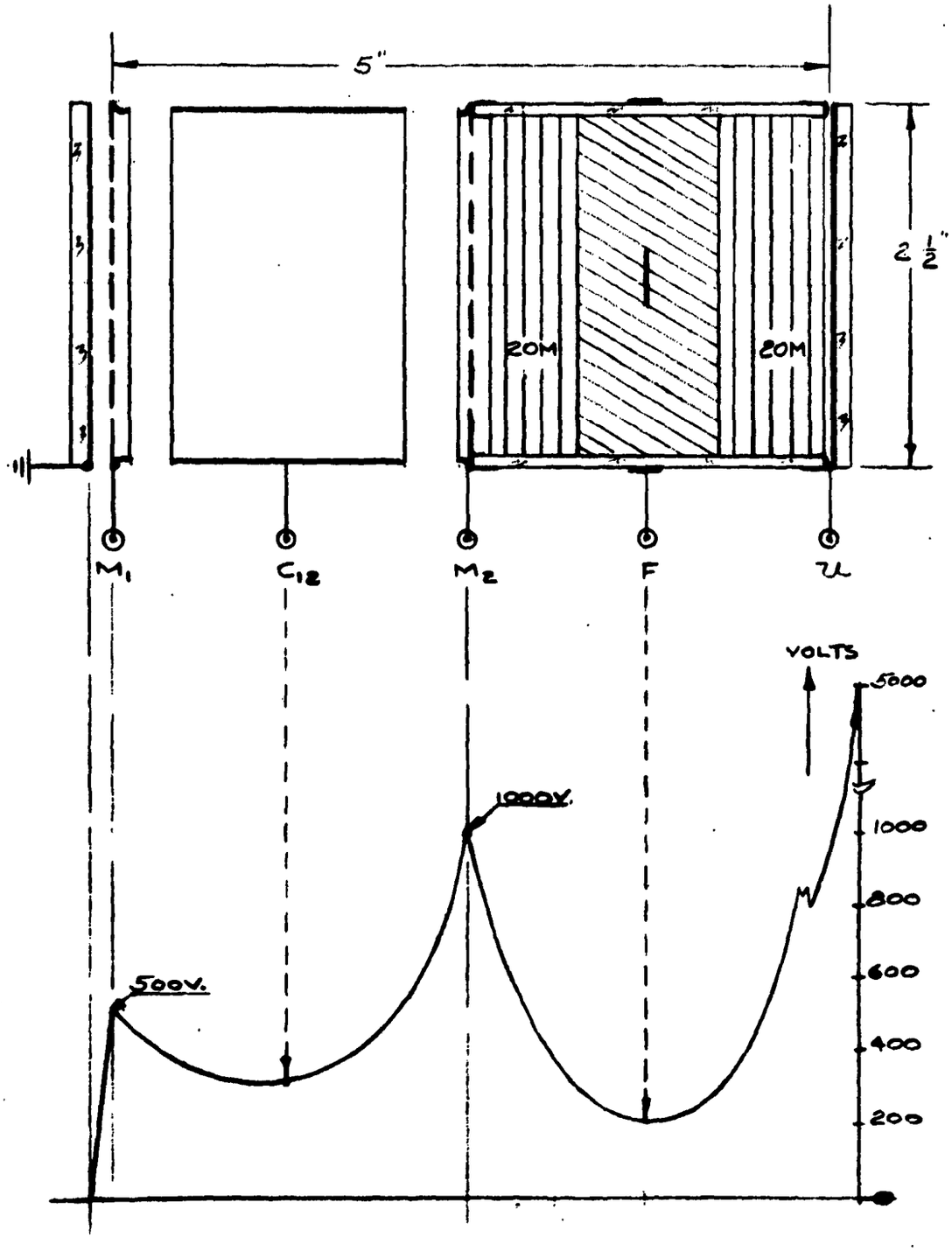

fig 3.14- A SYMMETRICAL LENS SYSTEM

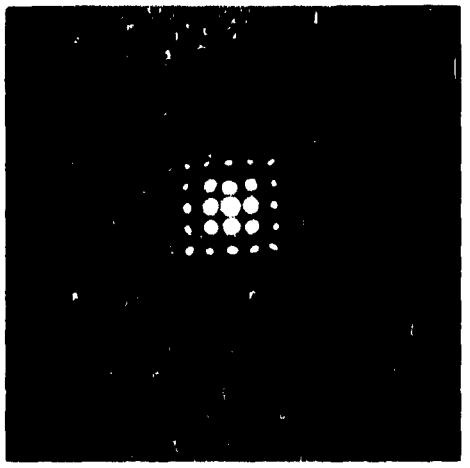

3.15a.

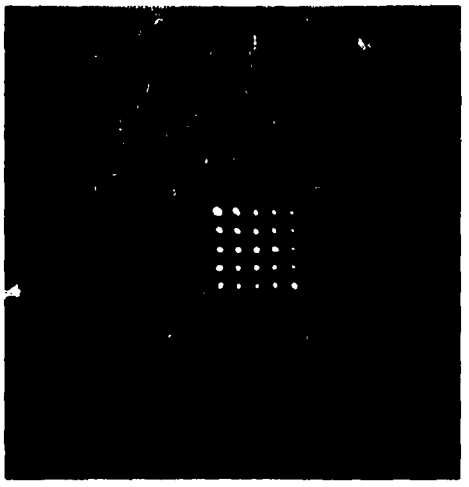

3.15b.

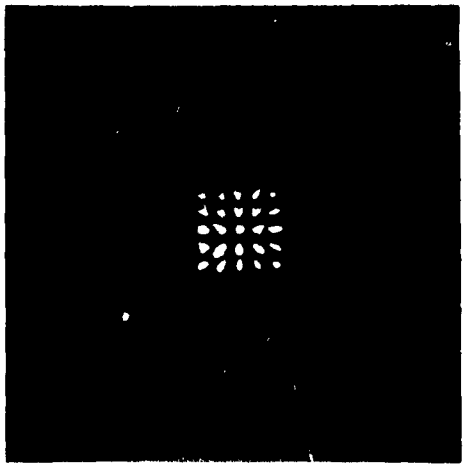

3.15c.

Figure 3.15- Field Correction by a Lens Doublet

3.15-b, the sides of the square are straight, whereas they are barrelling in 3.15-a and pincushioning in 3.15-c.

In photography, there exists a very close analog to the electron-optics considered here. It is called "orthoscopic doublet". This photographic objective consists of two symmetrical, positive lens elements, spaced far enough apart so that a crossover occurs between them. A center-stop permits the passage of rays near axis and rejects all others.[23)]

A system of this kind is called "orthoscopic" because it achieves correction of geometric distortion.

In the present electron-optics, the same effect occurs. However, it is found here that other distortions are being minimized, too. This includes curvature of field and astigmatism. It is of general interest to find that certain aberrations may be reduced in electron-optics, as well as in light optics, by the use of two lens sections in tandem.

As to actual performance, the orthoscopic system with plane meshes was judged inferior to the plano-convex system in four respects:

1. The maximum focused area was smaller in a tube of given size (3/4" vs. 1-1/2" in 2-1/4" id).

2. Edge-focus performance was inferior since residual coma remained uncorrected (for comparison, see photograph 4.6, Section 4).

3. Adjustment was critical; mode switching occurred within $\pm$ 12 per cent of focus voltage.

4. The overall magnification was too small for present purposes ($m = 0.42$ versus $m = 0.67$).

It therefore was decided to continue the use of the hyper-convex field mesh for all further work on the contract. Its higher cost seemed well-justified by its superior performance.

4. IMAGE TUBE WITH ONE SPIRAL LENS

A Demountable Experiments

The field flattener shown in Figure 3.9 was tested in an image-tube gun shown in Figure 4.1. This tube used one spiral lens and two meshes (M_1 and M_2). The spiral lens was located between the cathode-lens section and the spiral-accelerator section. The input to the lens was covered by the convex field mesh M_2, but the lens output at the junction J to the accelerator section was left open.

Figure 4.2 shows a photo of this tube. It measured 2-1/2" by 8".

Table IV-A shows some typical voltage levels used.

TABLE IV-A

Single-Lens Tube: Data

	M_1	C_1	C_2	M_2	B	J	U	Magnification
Voltage	50	50	230	740	510	740	7500	0.67

Note that the focusing sections operate at relatively low voltages (1000 volts or less). Normally, the spiral lens was used in a non-accelerating mode; i.e., the terminals M_2 and J were at the same voltage. In this case, the tube had a fixed magnification of 0.67:1. In a later test, the shunt from J to M_2 was replaced by a variable resistor R_2, allowing the potential of M_2 to fall below that of the junction J. This action permitted a slight reduction of magnification, from a value of 0.67:1 to about 0.5:1. In the circuit shown in Figure 4.1, focus and image geometry were practically unaffected by this change of scale.

On the other hand, changes of the voltage distribution in the cathode-lens section had a pronounced effect on geometry and edge-focus. Figure 4.3 shows a set of three conditions, observed with a variation of the C_2-bias alone. Typically, moving this voltage from 240 through 280 to 340 volts caused a transition from barrel, through square, to pincushion geometry, as shown in the photographs.

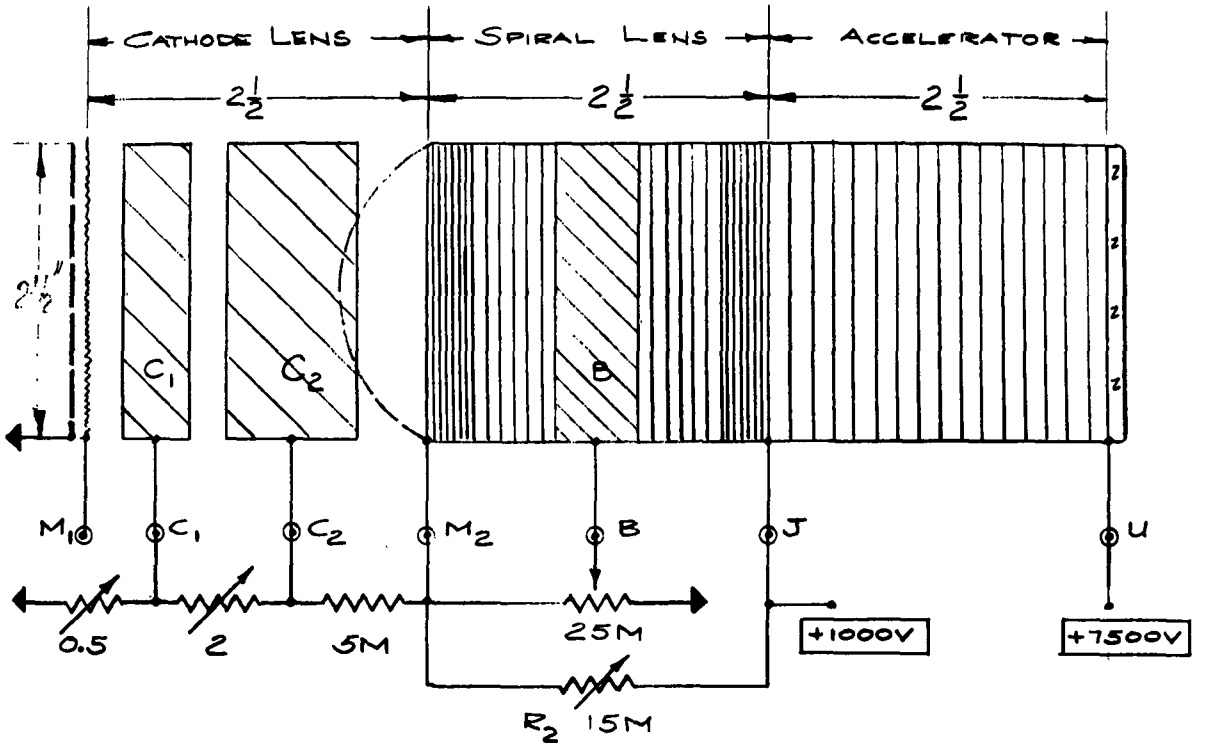

Fig. 4.1: Single Spiral-Lens Tube

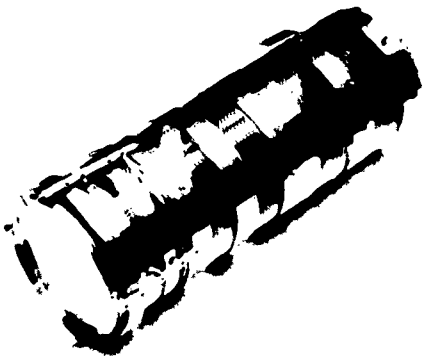

Fig. 4.2: Photograph of

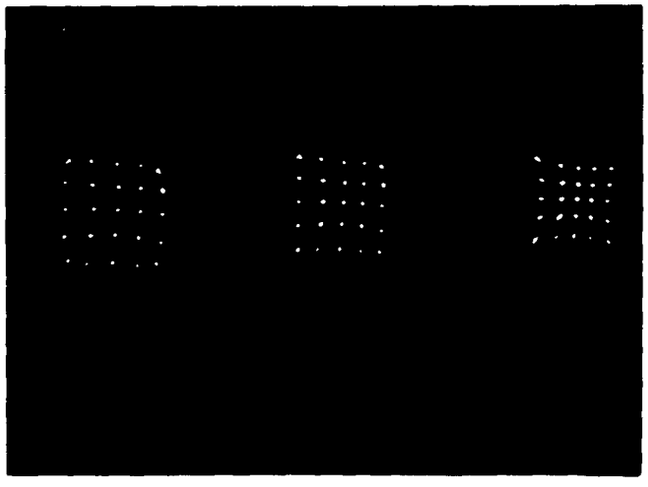

Figure 4.3: Correction of Field Geometry

4. IMAGE TUBE WITH ONE SPIRAL LENS (Continued)

It was concluded that the cathode-lens section should be required only to adjust for optimum geometry and flatness of field. Control of magnification and image size should be accomplished in the spiral lens-section, following the cathode-lens. This plan prompted the subsequent development of image tubes with Zoom-lens action, which will be described in a later section (Section 5).

B. Sealed-Off "Fixed-M" Tube

Following up on results gained from thermionic analogs in the demountable, a scale-model of the preferred type of analog was built into a sealed-off image tube. This tube had a single spiral lens and yielded essentially fixed magnification. Figure 4.4 shows this "fixed-M" type tube. It had an S-9 flat photocathode on one end of a 2-1/2" x 6" envelope and a flat P-20 fine-grain screen on the other end.

Figure 4.5 shows a 1-to-1 cutup of the same tube, along with the voltages used for optimum operation. It is seen that the tube uses one cathode-lens section and one spiral-lens section. Both sections are separated by a hyperconvex mesh M_2, which acts as an internal field flattener (see Section 3, Figure 3.9).

Immediately after leaving the cathode, photoelectrons are accelerated strongly by the plane mesh M_1 (90 lines per mesh, 90-per-cent transmission), which is stretched 1/8" behind cathode. It can be shown that photoemission from each point on K then is confined within a cone with half-angle α, where:

$$\alpha = \sqrt{\frac{e_o}{E_1}}$$

Here, e_o is the peak emission velocity; and E_1, the mesh-voltage. With $e_o = 1$ volt, and $E_1 = 1200$ volts, we find

$$\alpha = 1.7^\circ$$

It can be shown that these pencils cover more than one elemental area on the field-mesh M_2, so that no more than 200 l.p.i. are required there. On the other hand, for the first mesh M_1, a higher resolution than that used here would be advantageous.

Figure 4.6 shows a typical result obtained with this tube. The small picture is to scale; the large photograph is blown up by 3:1. The fine texture seen within each dot is the cathode-mesh. It had a grid spacing of 10 mils and a wire diameter of less than 1 mil.

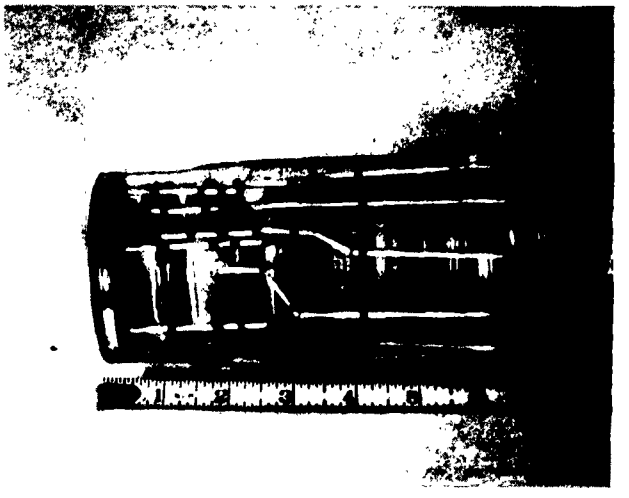

Fig. 4.4- IMAGE CONVERTER WITH FIXED MAGNIFICATION

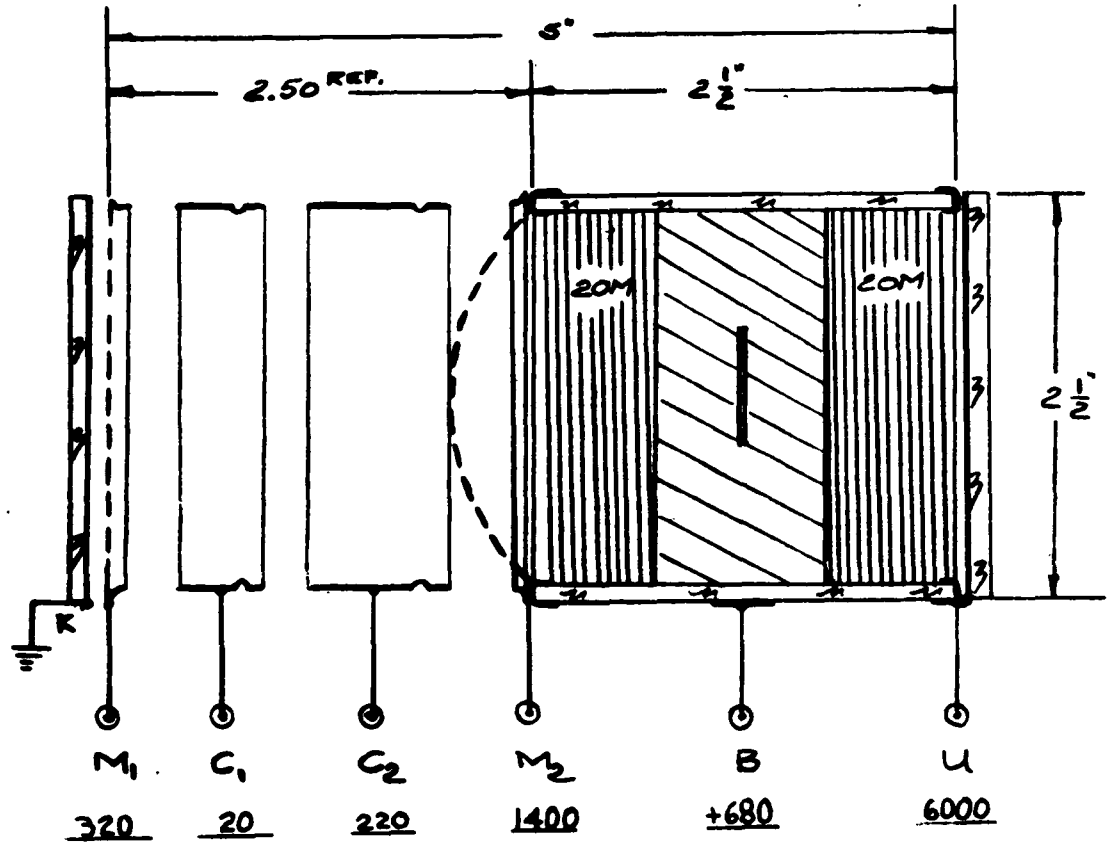

fig. 4.5- IMAGE CONVERTER FOR FIXED MAGNIFICATION

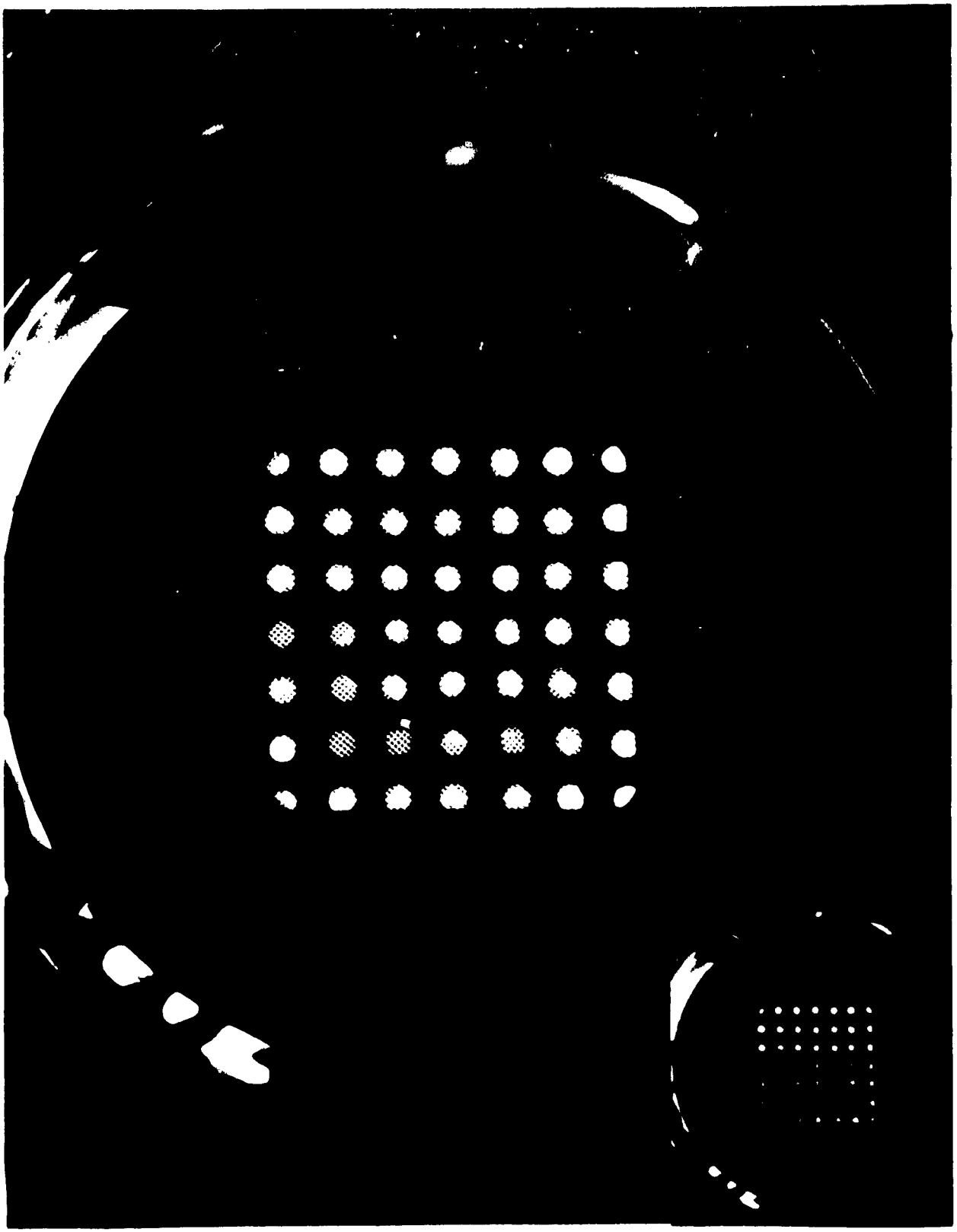

Fig. 4.6- IMAGE OBTAINED WITH CONVERTER TUBE OF Fig 4.4

4. IMAGE TUBE WITH ONE SPIRAL LENS (Continued)

This texture may be recognized across the entire picture area, indicating a practically flat field of focus and good edge resolution.

Geometric distortion is virtually nil. Quite generally, this could be influenced by voltages applied to the ring-electrodes C_1 and C_2. In actual practice, it was found that optimum geometry could often be obtained with both rings at the same voltage (-100 volts). The resulting simplified tube assembly is shown in Figure 4.7.

Magnification was 0.8 for U = 3400 volts; and 1-to-1 for U = 2000 volts.

In these tests, the optical image projected on cathode had a diagonal of 1-1/2", thus filling 75 per cent of the 2"-cathode diameter.

The electron-image had a diagonal of 1-1/4" at U = 3000 volts. This size increased with decreasing ultor voltage, until it filled about 85 per cent of the screen diameter at 2000 volts. Distortion did not seem to increase in the process. Unfortunately, at 2000 volts, light output was too low for photographic purposes.

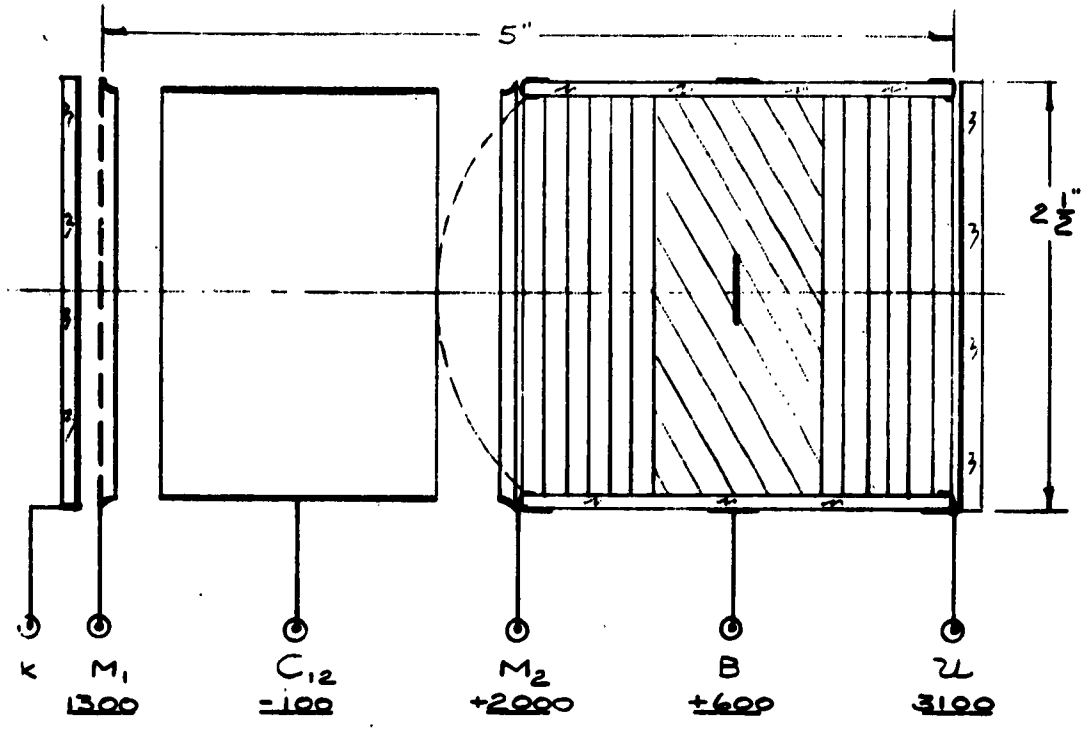

fig. 4.7- FIXED-M IMAGE CONVERTER: CATHODE-LENS SECTION SIMPLIFIED

5. TWO-SPIRAL-LENS TUBE (ZOOM-LENS)

A. Thermionic Analog

The results obtained with the one-lens spiral tube encouraged work on a two-lens system, henceforth referred to as a "Zoom-lens" tube. Theoretical analysis by Electron Trigonometry had indicated that this type of spiral-optics should be capable of magnification control over a range of more than 7:1.

An appearance-photo of the thermionic analog is given in Figure 5.1; and a cross section of it in Figure 5.2. The field-flattener section in this two-lens tube is the same as that used in the one-lens tube (Section 4). The focusing section, however, now employs two, rather than one, non-accelerating spiral lens units, joined together at the junction J and presenting two focusing electrodes B_1 and B_2, respectively. No mesh is used at the junction J; but the double-lens unit, which is 5" long, is covered at the input by the hyperconvex field mesh M_2, and at the output by a plane separator mesh M_3. The overall length of this first Zoomar-tube was 10-1/2". In a more recent version of the Zoomar-tube, the image section has been considerably shortened; and the sealed-off tube now measures only 8" in length (Figure 5.6).

1. General Principle of the Zoom-Lens Spiral

Action of the tandem spiral has been predicted correctly by Electron Trigonometry. Since the twin-lens section of Figure 5.2 is shielded at both ends by meshes, but is open in the center at J, the voltage gradient on axis must be continuous within the lens-section; but it may change abruptly at the boundaries. Accordingly, three distinct modes of operation are anticipated. These modes are introduced in Figure 5.2 as modes I through III, respectively. In mode I, the first spiral-band B_1 is depressed below, and the second spiral-band B_2 is raised above, an anode voltage V_a, which is common to both terminating meshes M_2 and M_3 at the lens boundaries. In modes I and III, this anode voltage is applied also to the center junction J.

In mode I, lens #1 is positive; and lens #2 is negative. As a result, the overall magnification is a maximum.

Figure 5.1: Zoom Lens Tube Structure

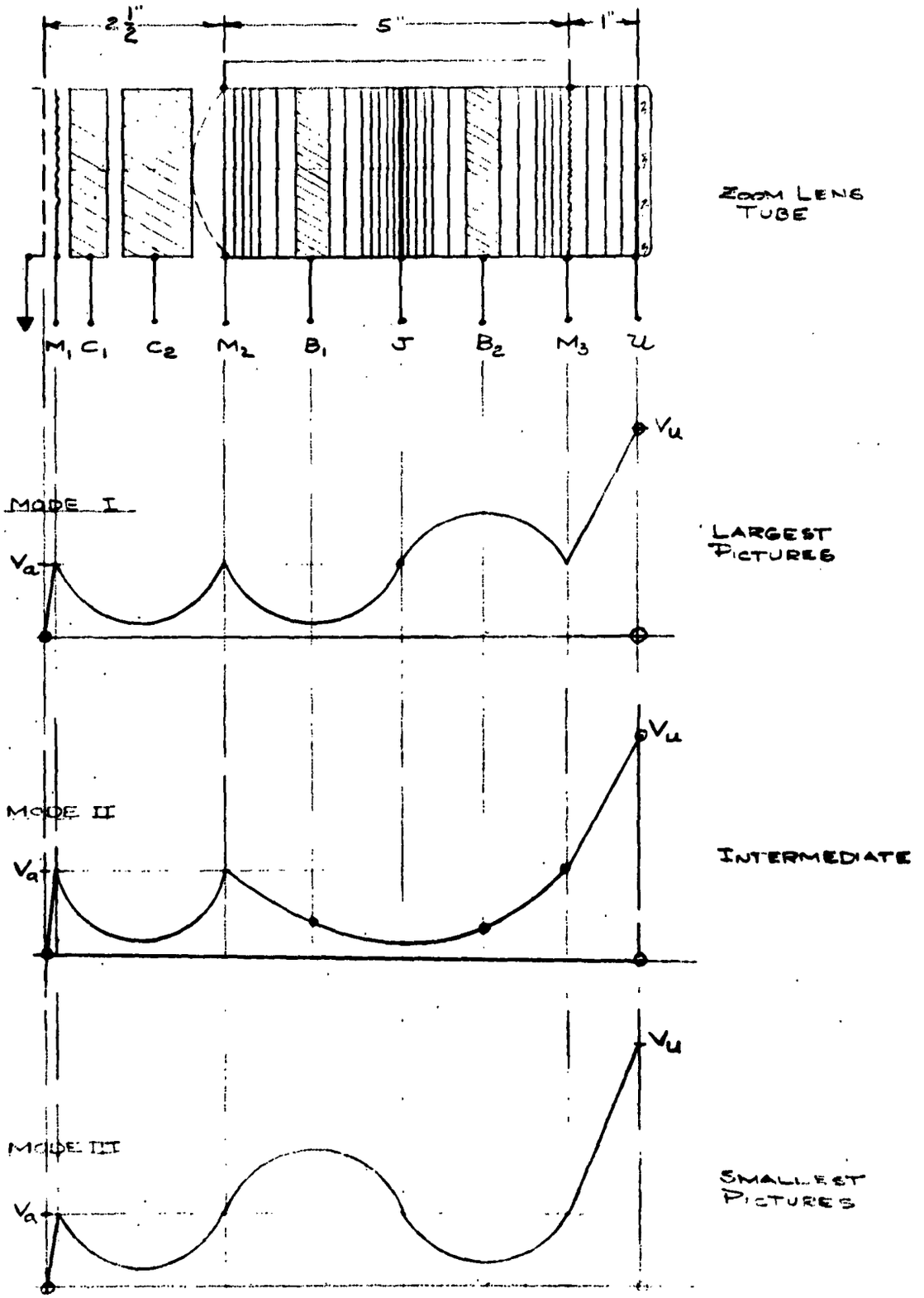

Fig. 5.2 - SPIRAL ZOOM LENS

5. TWO-SPIRAL-LENS TUBE (ZOOM -LENS) (Continued)

In mode III, this state of affairs is reversed. Lens #1 is negative, and lens #2 is positive. The net result is a minimum range of magnification.

In mode II, the junction J is depressed with respect to both M_2 and M_3, while both bands B_1 and B_2 are free to assume intermediate voltages. The entire Zoom-lens now acts like one long, positive lens. It thus may be expected that mode II will yield images on a scale intermediate between modes I and III.

2. Theory of the Zoom-Lens

A detailed analysis of this configuration has been performed by Electron Trigonometry. This computation was done for a tube with slightly different dimensions. assuming a Zoom-lens section of 2 x 2" length, mounted between an object- and image-throw of 1" and 2", respectively. Results of this analysis are given below:

TABLE V-A

Zoom-Lens: Theoretical Data

Mode	Lens #1	Function	Lens #2	Magnification
I	+360V	1,000 V	+1,160	-2.73
III	+1,500V	1,000 V	+ 300	-0.35

Mode #2 has not been calculated.

Table V-A indicates that a Zoom range as high as 7.5-to-1 may be realized with a two-spiral lens under certain conditions. The actual value of this ratio depends, of course, also on optical dimensions outside of the Zoom-lens. This includes the image throw. In general, with a given object-distance, the Zoom-ratio will increase with decreasing image distance; and vice versa.

5. TWO-SPIRAL-LENS TUBE (ZOOM-LENS) (Continued)

In addition, the above analysis indicated that the three modes of operation of the two-spiral lens will be discontinuous, rather than transitional. In practice, this would imply that a system such as Figure 5.2 will permit essentially three discrete adjustments; one for high, medium, and low magnification, respectively. This, however, holds only for the non-accelerating type of Zoom-lens shown ($M_2 = M_3$).

If different voltage levels are admitted to M_2 and M_3, it is conceivable that a more flexible range of adjustments may be observed, similar to experience reported for the one-spiral tube.

3. Experimental Test of Zoom-Lens Analog

Experiments with the Zoom-lens spiral largely have verified the above analysis. Figure 5.3 shows a typical result obtained with the tube shown in Figure 5.1. The three conditions shown differ in magnification by the ratio of 4:2:1. Note also the fact that the field of view includes 21 of the 25 dots in the object**, representing 83 percent of the total cathode area, or 2.1" out of an inside-tube diameter of 2.5".

Table V-B shows typical voltage values as they were used to adjust the three conditions of Figure 5.3. Again the Zoom-lens section runs on a low average voltage (500 volts). Deviations of M_2M_3 voltages from 500 volts were incidental. The ultor voltage had no influence on image size. Negative voltages have since been eliminated.

4. Open-Ended Zoom-Lens

The above tube used three internal meshes (Figure 5.2). Attempts were made to reduce this number by one. In a subsequent test, mesh M_3 at the Zoom-lens output was removed. It was, of course, anticipated that this would reduce greatly the Zoom-ratio, especially in mode I, which calls for a discontinuity of field at the lens output. This condition, therefore, no longer can be realized in the absence of the mesh M_3.

** Note that the holes in the cathode-plane measure 0.062" in diameter. See Figure 2.1 in Section 2.

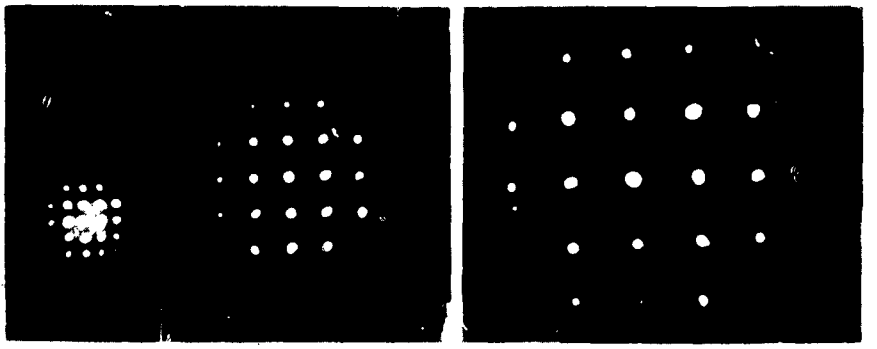

Figure 5.3: Performance of the Shielded Zoom Lens

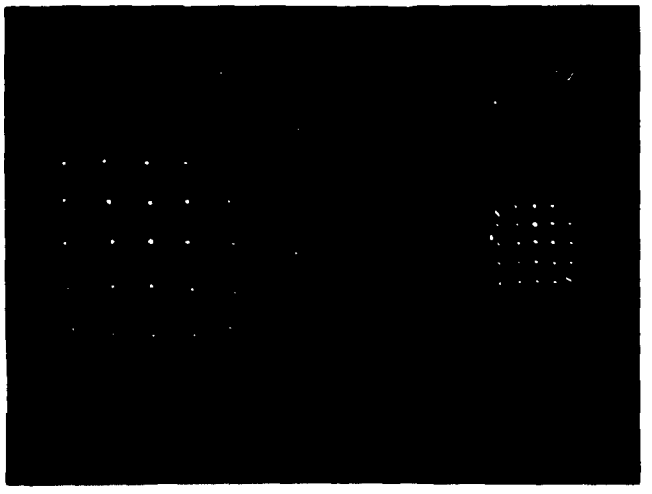

Figure 5.4: Performance of the Un-Shielded Zoom Lens

TABLE V-B

Typical Adjustments For Zoom-Lens Tube of Figure 5.1

Mode	K	M_1	C_1	C_2	M_2	B_1	J	B_2	M_3	U	Dot Spacing	Magnification
I	0	100	120	260	460	+180	460	1,000	460	7,500	1/2"	1.33
II	0	100	120	310	570	220	-130	220	570	7,500	1/4"	0.67
III	0	100	150	320	580	960	580	+60	580	7,500	1/8"	0.33

Experience has borne this out, as shown by Figure 5.4. Resolution seems to be improved by the absence of a third mesh. However, the total Zoom-range is now much smaller; viz., 2.3:1, as compared to 4:1 with the shielded tube. The highest value of m corresponds roughly to the intermediate value, formerly obtained in mode II with the triple-mesh tube. The large-scale images realized before in mode I are no longer realizable with the two-mesh tube.

B. Sealed-Off Image Converter with Zoom Lens

To demonstrate the capabilities of composite spiral-optics, a sealed-off image converter with controlled magnification was built. Figure 5.5 shows a photograph of this tube with Spiral-Zoom lens. The gun assembly measured 2-1/2" x 8-1/2". This tube is two times up from the dimensions of a standard image converter triode (type 6032), which has almost the same aspect ratio (2.8 vs. 3.4).

As Figure 5.6 shows, the Zoom-lens tube has the same field-flattener structure as the fixed-m-type tube (Figure 4.5). This includes a first-anode mesh M_1, the two ring electrodes C_1 and C_2, and the hyperconvex field mesh M_2.

In the focusing section, we recognize a 2-1/2" by 5" glass cylinder, supporting two, rather than one, spiral-lens units in tandem. Their respective focus electrodes are brought out at B_1 and B_2. The ends of the cylinder are terminated by meshes M_2 (convex) and M_3 (plane), both of medium resolution (90 and 110 l.p.i.) and high transparency (95 percent each). M_2 and M_3 always are connected together; but the junction J is connected, either to the same voltage as M_2M_3, or to a separate focus voltage.

Figure 5.7 shows a schematic of the power supply for this tube. A three-pole, three-position wafer switch is used to apply, to the Zoom-lens, pre-set focus voltages from the potentiometers F_a, F_b, and F_c. The remaining switch functions are such as to generate, along the Zoom-lens, three distinct modes of voltage distribution, in line with Figure 5.2.

Fig 6.5:- IMAGE CONVERTER WITH SPIRAL-ZOOM LENS

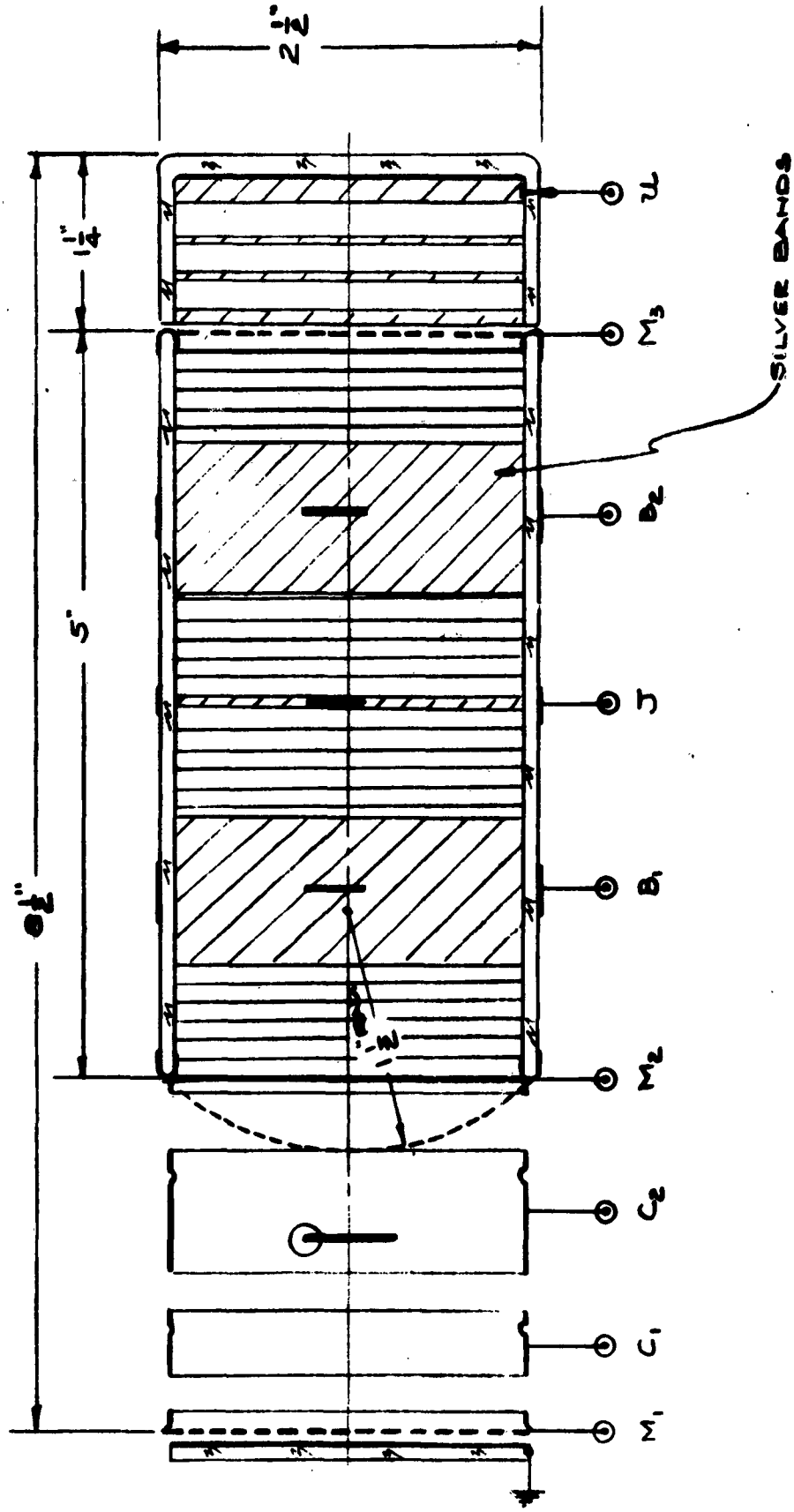

fig. 5.6 - Cross-Section of Zoom Tube

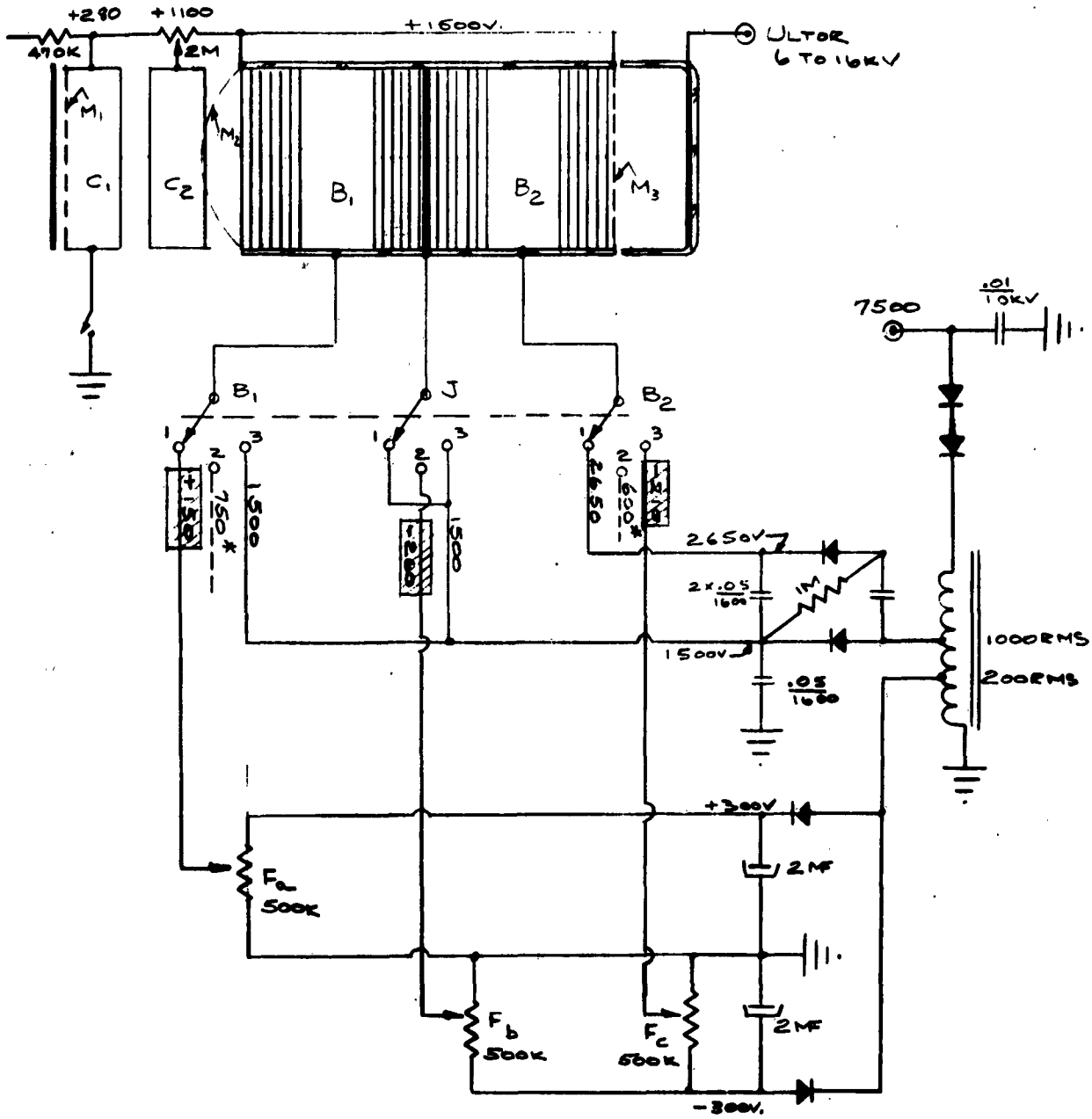

NOTE -

* SELF SETTING VOLTAGES, DETERMINED BY SPIRAL RESISTANCES

fig 5.7 - POWER SUPPLY FOR ZOOM TUBE

5. TWO-SPIRAL-LENS TUBE (ZOOM-LENS) (Continued)

The actual results obtained are shown in Figure 5.8. Data on magnification observed in the three modes are listed below:

TABLE V-C

Zoom-Lens Action

Condition	Magnification	Zoom Range
I	3/2	4.5
II	3/4	2.25
III	1/3	1

It is noteworthy that the ultor voltage did not have any influence on picture size. This made it possible to change screen voltage in such a manner that image brightness stayed constant regardless of size! If this was not done, the smallest image far exceeded the largest one in luminance.

Stop Motion Operation

Contrary to the previous tube type, the Zoom-lens was operated with M_1 at a relatively low voltage (180 volts). While this degraded resolution to some extent, it offered a facility to use M_1 as a shutter electrode. All three conditions shown in Figure 5.8 could be switched on and off by a voltage pulse of 200 volts.

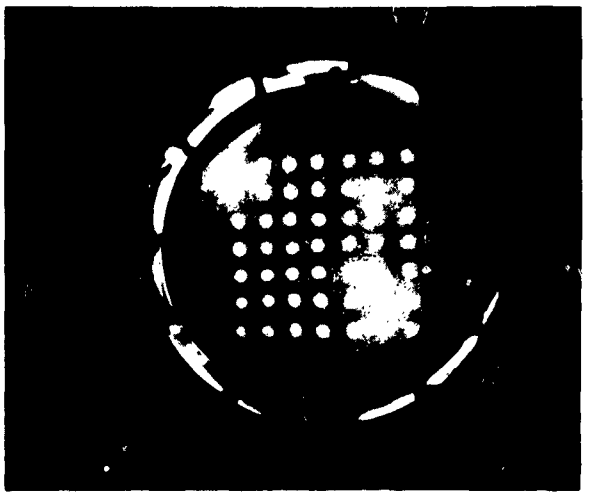

5.8a.

5.8b.

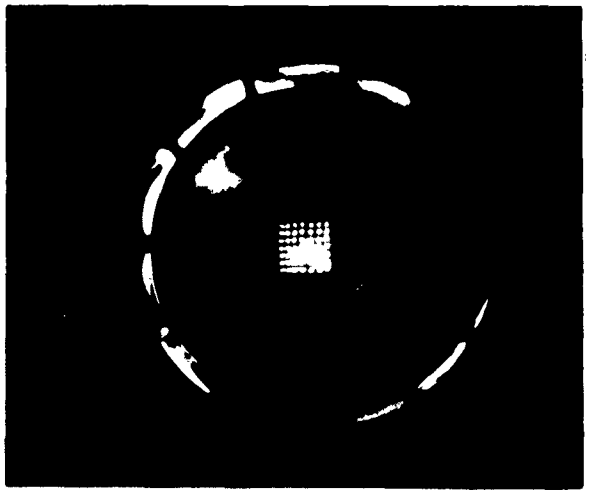

5.8c.

Fig. 5.8 - Zoom Lens Action

6. VOLTAGE-SENSITIVE ELECTRON-OPTICS

A. Introduction

Toward the end of the contract period, a time-limited effort was made to develop electron-optics for direct visual display of a voltage distribution. This problem is related closely to the development of an image-converter for thermal radiation beyond 1μ. Since photoemission ceases around 10,000A, conventional image converters become inoperative there.

In the infrared spectrum beyond 1μ, current-sensitive electron-optics must be replaced by a voltage-sensitive type. Photovoltaic materials can develop an electromotive force (EMF) directly under infrared radiation. Much higher signal voltages (10 to 20 volts) can be realized with photoconductors, if the principle of charge storage is utilized. Typical examples for both types of materials are listed below[24]:

TABLE VI-A

Semiconductive Materials for IR Targets

Detector	Material	Long-Wave Limit	Cooling Temperature	Storage
Photovoltaic	Indium-Antimonide	$\lambda = 5.5\mu$	77°K	No
Photoconductive	Germanium-Silicon Alloy, Gold Doped	$\lambda = 8 + 14\mu$	50°K	Yes

In either case, the electron-optics for the display of a charge-image must be "voltage-sensitive". By contrast, the electron optics used in conventional image converters are "current-sensitive".

Since there is no inherent photoemission from the target, a separate source of electrons must be used. In conventional camera tubes of the "Vidicon" type, this source is a focused beam, scanning the target. The output signal then is <u>electrical</u>, rather than optical. Its display requires the complex equipment found in a video-camera chain.

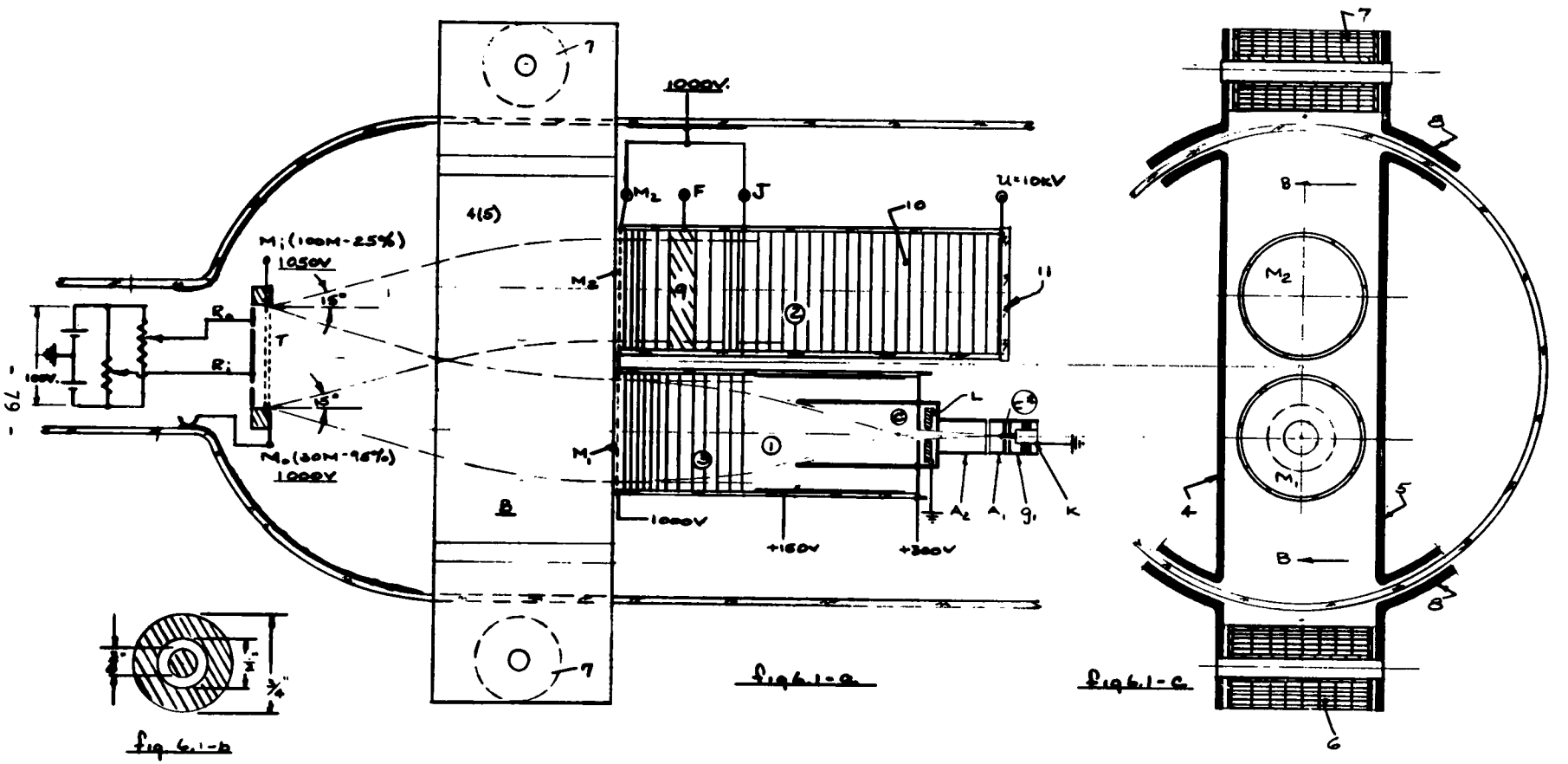

fig. 6.1- Voltage-Sensitive Image Converter with inclined reflective El. Optics

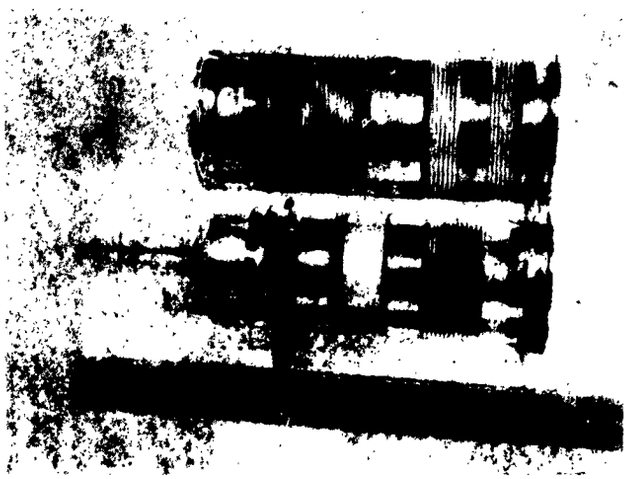

Fig. 6.2 - REFLECTIVE OPTICS WITH PARALLEL GUNS

6. VOLTAGE-SENSITIVE ELECTRON-OPTICS (Continued)

Considerable simplification is possible by the development of a non-scanning camera with optical, rather than electrical, output. In this type of camera, focused scanning-beams are replaced by a broad floodbeam, which is stationary in the tube.

B. Reflective Optics With Tilted Beam

Design problems are simplified, if the floodbeam illuminating the target is well-collimated. A suitable electron-optical system, using resistive spirals, has been described in Section 2 of this report. The same system was used as a source for flood-electrons in the first camera tube, which is shown in Figure 6.1. This tube had parallel gun barrels, but used skew incidence of beams on target.

Figure 6.1-a shows the paraxial arrangement of floodgun (1) and viewing-gun (2). This assembly is illustrated further in the photograph, Figure 6.2. Both guns are employing spiral-optics. The floodgun uses an accelerating type of spiral lens (3), which collimates a conical beam by accelerating it from 300 volts at apex (C) to 1,000 volts at the output-mesh (M_1) (90 lines per inch, 90-percent transmission). Point C is the real image of a crossover (C*) near cathode (K). To form this image at (C), the center element (L) of the Einzel lens is grounded.

The parallel floodbeam of 1,000-volt electrons is bent through 15° in a uniform, magnetic sorting field (B). After leaving (B), the beam illuminates a simulated target (T), centered on the axis of the envelope.

More detail of the simulated target is shown in Figure 6.1-b. It consisted of a system of two meshes, M_o and M_i, covering two co-planar, and concentric, rings R_o and R_i. Of the two meshes, the outer one (M_o) had low resolution (30m) and high transmission (95 percent) and was at Dag-voltage (1,000 V). The inner mesh (M_i) had medium resolution (100m) and low transmission (25 percent) and was slightly more positive than M_o (+1,050 V). In this arrangement, M_o acted as a repeller for secondaries from M_i.

The two concentric rings R_o and R_i were brought out, separately. By applying near-ground bias voltages to each, various simple charge distributions could be simulated.

6. VOLTAGE-SENSITIVE ELECTRON-OPTICS (Continued)

With a positive bias on R, beams were absorbed on target (destructive viewing). With zero, or negative, bias on R, beams were reflected from target under $-\alpha$ where α is the angle of incidence on target (non-destructive viewing). The reflected beams were caught in the viewing gun (2), which they reached through mesh M_2 (identical with M_1) after being re-directed parallel to axis by the sorting field B.

Figure 6.1-c shows a front view of the plane through M_1 and M_2. The magnetic sorting field B was uniform and normal to the plane through the axes of both gun barrels. It was generated between two plane-parallel mu-metal strips 4,5. These strips were in magnetic contact with two bobbins 6,7 through flanges (8) on both sides of the glass-wall.

The viewing gun (2) consisted of a non-accelerating spiral lens (9), wound as a two-step approximation to a parabola (see Section 1). Focusing was done on the center-band F, with M_2 and J interconnected at 1,000 volts. The linear-spiral section (10) served as an intensifier for the electron-image of T, formed by the spiral-lens (9) at a low voltage (1,000 V) and short throw. This image then was displayed on the screen (11) at high voltage (U = 10KV). Figure 6.2 shows a photograph of the completed parallel-gun assembly, minus target and magnet.

C. Two Modes of Operation

When this test was planned, two possible modes of operation were anticipated:

I: destructive readout
II: non-destructive readout

In Mode I, flood electrons are reflected from negative, but land on positive, target areas. The target-image formed by return electrons is a "negative"; i.e., dark for positive and bright for negative, target areas. This Mode I operation is destructive to free positive charges on target.

In Mode II, average target potential is lowered such that electrons never land. Picture information is picked up by the return beam when it comes close to the charge image on target. This happens as follows:

A multitude of individual pencils is cut out of the floodbeam by the holes in the (inner) mask M_1. Each one

of these pencils describes a parabolic path in the space between M_i and T, before it leaves the interaction space through another hole in M_i. However, the ray will hit, or miss, that exit-hole, depending on the deformation of its path by the charge seen on target. As a result, both positive and negative return-beam images should appear alternately, as the average target bias is varied.

D. Test Results with Tilted-Beam Tube

The round-trip beam path from floodgun through target to viewing screen functioned well, once the sorting field was adjusted for proper amplitude and direction. Direct crosstalk between guns was absent. However, Mode II could not be realized.

Mode I was found. A negative image of R_o and R_i appeared; and either ring could be switched on and off, individually. Magnification was too small for convenient viewing (m = 1/3). Voltage sensitivity was too small, and cutoff required +80 volts. Peak light output occurred with the target at zero bias. Resolution was poor (8 lines per inch).

E. Reflective Optics with Normal Incidence

Much better results were obtained with a second test, using a structure as shown in Figure 6.3. In this tube, beam incidence on target was normal, but both floodgun and viewing gun were tilted by $\pm 20°$ off-normal. An external, anastigmatic deflection yoke[25] was used to bend beams into - and out of - the axis of symmetry.

The target was similar to the one used before; however, the outer mesh (M_o) was omitted. The inner mesh M_i had the same resolution (100 mesh), but higher transmission (50 percent), than was used before. The floodgun was simplified by using only one crossover (near cathode). Floodbeam diameter was reduced from 2" to 1". Readout-magnification was increased four times, by increasing the length of the spiral accelerator, and by reducing the object distance.

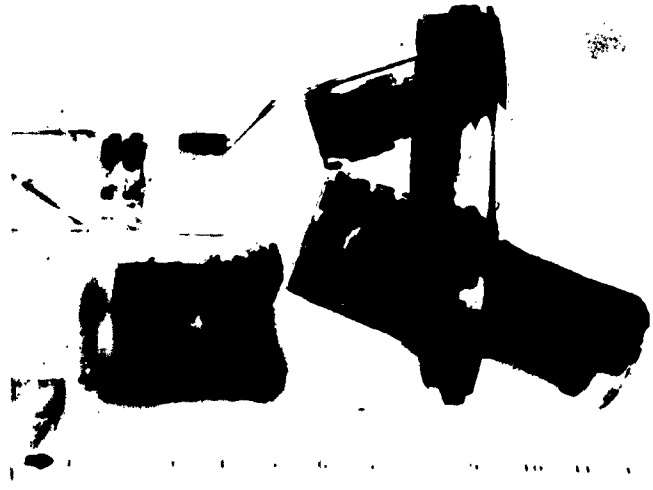

Fig. 6.3- REFLECTIVE OPTICS WITH INCLINED GUNS

6. VOLTAGE-SENSITIVE ELECTRON-OPTICS (Continued)

F. Results with Tube II

With normal beam incidence, only a mode I-type of operation was expected. This mode was observed.

Figure 6.4 shows photographs of typical images seen. The three conditions shown were obtained, respectively, by applying voltages of +110 or +140 volts to the two concentric target electrodes R_o and R_i, in various combinations. Resolution is commensurate with the mesh resolution employed (100 l.p.i.). Target voltage covered a range of 30-to-40 volts for full modulation of image intensity.

Elliptic distortion was in evidence. The minor axis lay in the plane defined by both guns. The ellipticity observed checks with the perspective of the target as viewed by the read-gun. Over-all magnification was 1.33. Picture brightness was good.

6.4a

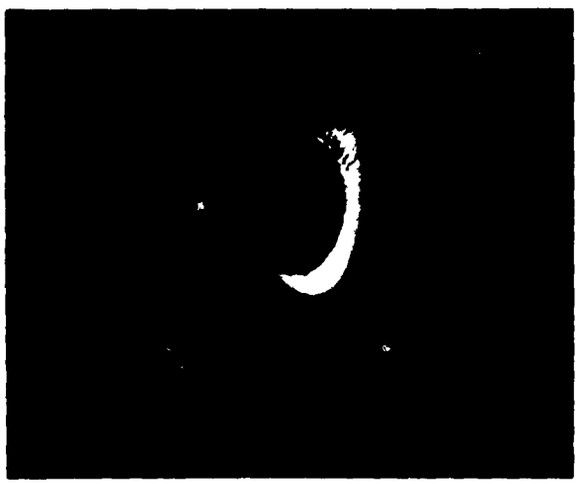

6.4b

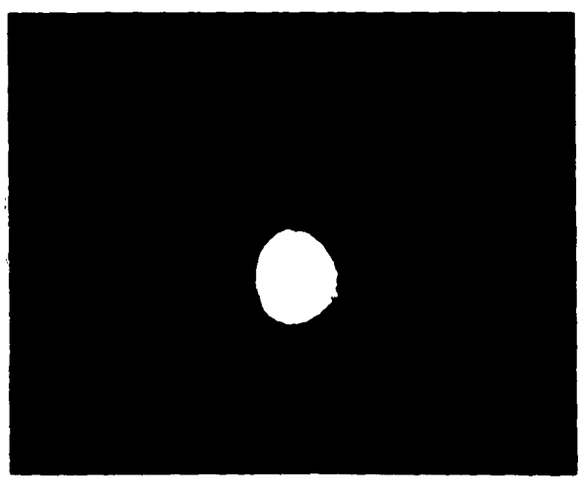

6.4c

Fig. 6.4- Electron Images By Reflection

7. PROCESSING TECHNIQUES

A. Introduction

Two electron-focusing geometries were evaluated in a demountable system wherein the source electrons were from a thermionic floodbeam apertured by a cathode-plate. The two geometries are a Zoom-lens tube shown in Figure 5.6 and a fixed demagnification tube shown in Figure 4.5. In order to evaluate the electron focusing geometries for use in photoemissive imaging devices, it was necessary to determine experimentally the focusing characteristics with source electrons from a typical photoemissive surface in a sealed-off tube.

B. Sealed-Off Tube Design

A two-piece envelope was designed with the necessary number of leads to permit processing and operation of the Zoom-lens configuration. After mounting the pre-assembled focusing structure into the larger envelope section, the two sections of the envelope were joined by inert gas welding of Kovar flanges. The envelope has exhaust tubulation from the side through which the tube is pumped during bakeout and photocathode processing.

A similar envelope was made for the fixed demagnification tube. Since this structure required fewer pin connections than the Zoom-lens tube, another envelope was designed, using the seven-pin image stem of the image orthicon. The two sections of this envelope were joined by a glass-to-glass seal.

The photoemissive surface chosen for the sealed-off tubes was an S-9, a semi-transparent layer of cesium antimony. This surface was chosen as the simplest to process in this structure and still yield the experimental information desired. In order to use the previously made cathode-lens parts and geometries, no changes were made to provide an internal source of antimony as is generally done in mkaing the S-9 photosurface. Instead, the antimony evaporation was made onto the faceplate end of the tube envelope in a bell-jar vacuum system. The envelope then was removed, and the internal focusing structure was inserted and welded to the envelope leads. The two portions of the envelope were joined along the Kovar flanges by a heliarc-type weld. The tube then was put onto a pump station for bake-out and photocathode processing.

7. PROCESSING TECHNIQUES (Continued)

C. Processing of Sealed-Off Tubes

The following sealed-off tubes were processed successfully during the course of this program:

TUBE NO. 1

The first sealed-off tube successfully processed was a Zoom-lens tube. This tube has a P-1 screen and non-coated spirals. The rings in the screen cup were coated.

TUBE NO. 2

The second sealed-off tube processed was a fixed demagnification tube. This tube has a fine-grain P-20 screen and non-coated spirals. This tube utilized the envelope design wherein the two sections were joined by a glass-to-glass seal.

TUBE NO. 3

The third sealed-off tube processed was a fixed demagnification tube. This tube has a fine-grain P-20 screen and non-coated spirals. This tube differed from the second tube only with respect to tube envelope and a modified corona shield.

TUBE NO. 4

The fourth sealed-off tube processed was a Zoom-lens tube. This tube has a fine-grain P-20 screen and is the only tube in which coated spirals were used.

Several attempts were made before the first Zoom-lens tube was successfully processed. Among the initial difficulties encountered were inadequate cesium yield; open getter circuits; and shorts, opens, and excessive leakage currents in the photocathode monitoring circuit. As a result of these difficulties, several changes were made, including the relocation of cesium channels and the addition of extra channels.

A P-1 screen was used in the first tube because it was the only screened cup assembly available at the time the first Zoom-lens tube was made. In subsequent tubes, only fine-grain P-20 screens were used.

7. PROCESSING TECHNIQUES (Continued)

In all sealed-off tubes, an S-9, cesium-antimony, photoemissive surface was used. The photosensitivity in these tubes was relatively low, compared to the sensitivity of the conventional S-9 photosurface. The relatively low photosensitivity is attributed to the processing procedure adopted for these tubes. In conventional S-9 processing, an internal source is provided from which antimony is evaporated onto the photocathode substrate following bakeout of the tube. In these converter tubes, the antimony layer was deposited onto the photocathode substrate portion of the tube by a bell-jar vacuum evaporation prior to making the final envelope seal. This procedure permits the antimony layer to be exposed to air, the sealing environment, and the bakeout environment prior to reaction with cesium. It was anticipated that typical S-9 photosensitivity would not be obtained by this procedure; however, this procedure permitted the immediate assembly and processing of tubes without redesigning the front end of the tube to accommodate internal antimony beads. This procedure also avoided any problems that might arise in making the antimony evaporation through the first mesh. A gradual improvement of photosensitivity in successive tubes was observed. This improvement was attributed to better handling and cleaning of tube parts.

In the first three tubes made, the Dag spirals were uncoated. It was anticipated that cesium generated during photocathode activation would react with the exposed Dag spirals and reduce the resistance. The initial resistance of a spiral section in the first three tubes was in the range of 30 to 50 megohms. Following photocathode activation, the resistance of a spiral section had dropped 30 percent to 40 percent. It appears that the change resulting from exposure to cesium was uniform, since the change did not result in a deterioration of tube performance. It will, however, be necessary to keep this change in mind when designing a high-voltage spiral section to insure that the final resistance is sufficiently high to limit the power dissipated in the spiral.

In Interim Engineering Report No. 2, the use of spiral-coating techniques was described. The thin-film coatings described in this report have resistivities of the order of 10^{10} ohms per square. The advantages to be gained from coated spirals are the reduction of free charges from open glass areas and an improvement in high-voltage stability. After noting the drop in resistance of the Dag spirals after exposure to cesium, the possibility of using this coating to shield the Dag from cesium

7. PROCESSING TECHIQUES (Continued)

was considered. The fourth tube, a Zoom-lens configuration, was made with coated spirals. The resistance of each of the spirals before coating was approximately 50 megohms. Immediately following coating, the spiral resistance was still 50 megohms. Approximately three weeks passed between the time the spirals were coated and a tube was assembled. A measurement of spiral resistance after tube assembly indicated the resistance of a spiral section had dropped from the range of 50 megohms to 15 megohms. This assembly was sealed into an envelope and processed. After processing, the resistance of a spiral section was measured to be in the range of 150 thousand ohms. The resistance between the screen and the termination of the nearest spiral, which was initially of the order of 10^9 ohms, had dropped to the order of 10^6 ohms. As a result of this drastic change in spiral resistances, this tube was inoperable.

In the first operable sealed-off tube (a Zoom-lens configuration), uncoated spirals were used; however, the region between the termination of the last spiral and the P-1 screen was coated. The resistance of this element was originally of the order of 10^9 ohms. The resistance of this section is now approximately 45 megohms, which is still high enough to permit operation of the tube.

D. Summary and Conclusions

Two electron focusing configurations (a Zoom-lens structure and a fixed demagnification structure), employing a combination of meshes and non-linear spirals, were designed and evaluated in a bell-jar vacuum system. In this evaluation, source electrons were obtained from a floodbeam apertured by a cathode-plate. In order to evaluate these structures for use in photoemissive imaging devices, it was necessary to determine the performance with source electrons from a photoemissive surface.

Two Zoom-lens tubes and two fixed demagnification tubes were processed and sealed-off during this portion of the contract. An S-9, cesium-antimony-type photosurface was used in all sealed-off tubes. In the first tube processed, a P-1 screen was used; however, in the remaining tubes, a fine-grain P-20 screen was used.

The first three tubes processed used non-coated spirals. In the last tube (the second Zoom-lens type), coated spirals were tried. The last tube was inoperable, because of a drastic drop in resistance across each spiral section. The three sealed-off tubes with non-coated spirals were operable.

7. PROCESSING TECHNIQUES (Continued)

The following conclusions are based upon the limited experience gained from processing the four sealed-off tubes.

1. The lower-than-typical S-9 photosensitivity is attributed to processing and assembly procedures adopted for these tubes. This procedure permitted the immediate assembly of tubes, using parts made for the bell-jar evaluation and not designed with photocathode processing considerations in mind. The gradual improvement in photocathode sensitivity with successive tubes was attributed to better cleaning and handling of tube parts.

2. It was noted that the resistance of the non-coated Dag spirals used in the first three tubes dropped to about 60 percent of the initial value following exposure to cesium during the photocathode activations. It is concluded that the change in resistance was uniform along the spiral since it did not result in a deterioration of tube performance.

3. The drop in resistance across the coated spiral sections of the second Zoom-lens tube made the tube inoperable. A similar coating used between the termination of the spiral and the screen of the first Zoom-lens tube shows a drop in resistance insufficient to alter tube performance. Further investigations of the use of resistive spiral coating in these environments should be pursued in consideration of the benefits that might be obtained by their use.

8. CONCLUSIONS

It has been shown that plane-to-plane imagery by electrostatic electron optics is practical. In a typical image converter of this kind, useful object and image diagonals may occupy as much as 2/3 of the envelope diameter. This result is due to a combination of three circumstances:

1. Strong electron acceleration by a plane mesh anode adjacent to cathode.

2. Use of two, rather than one, electron-lens sections in tandem.

3. Use of a hyperconvex mesh as a boundary between the two sections.

In this lens doublet, the first section, or cathode-lens, acts as a field flattener, simulating a virtual cathode of convex shape. The second section acts as a focusing lens, projecting an image of this virtual convex cathode on the screen.

The independence of these two functions has been strikingly demonstrated by an image converter with Zoom-action. Here, the cathode lens section is left in a fixed adjustment, while the focusing lens section operates as a multiple-spiral lens with varifocal qualities.

It also has been demonstrated that this type of electrostatic electron-optics can give images from plane objects that are not capable of spontaneous electron emission but only of electron reflection. On this basis, one can develop electron-optical devices, employing photoconductive targets as storage elements, and using reflective electron-optics with a thermionic cathode to display the charge image on target.

9. FUTURE DEVELOPMENTS AND RECOMMENDATIONS

Results with plane-to-plane electron-imagery, using spiral lenses in combination with internal mesh modes, generally have been encouraging. It seems worthwhile, therefore, to aim at further improvement.

A. Image Converter

The fixed-in type of image converter may be improved in several respects. Higher resolution may be attempted by using higher voltages as M, and ultor and by employing more refined mesh texture where necessary.

The tube could be miniaturized to 1/2 or even 1/3 of its present size. This would be facilitated by the use of glass-to-metal seals, whereby a separate external envelope would be eliminated. The total pin-count could be reduced from 7 to 6, or even to 5, by interconnections, and by the use of electrodes with re-entrant shape. Such equivalent gun structures may be established in the electrolytic tank, while trying to duplicate the present field configuration.

Optical feed-through is somewhat of a problem at present. This can be much reduced by:

1. The use of a more efficient photocathode and

2. Depositing a heavier back-metal film on the screen.

The latter is feasible if higher ultor voltages are used (20 KV). In this connection, a separate, short, intensifier section with 10-to-1 post acceleration would be helpful.

B. Image Intensifier

The plane-to-plane feature of the new image converter lends itself to cascaded operation. A two-stage image intensifier appears possible using a screen-photocathode sandwich for coupling between successive stages. This type of device has been demonstrated successfully before using curved cathode surfaces*), The new planar geometry may yield an even better

---

*) Stoudenheimer and Moor, "Developmental Two-Stage Electron Image Converter", Image Intensifier Symposium, October 6-7, 1958.

9. FUTURE DEVELOPMENTS AND RECOMMENDATIONS (Continued)

center-to-edge ratio, besides facilitating the production of thin-film electrodes.

C. Zoom-Lens Converter

The Zoom-lens converter may be improved further by the following developments:

1) A continuous Zoom-lens with increased range (8-to-1).

2) A constant-size image displaying Zoom-action.

3) A Zoom-converter with coupled intensifier, yielding images of constant size and intensity.

4) Addition of stop-motion switching to a combination of the above features.

D. Voltage-Sensitive Image Converter

This device had to be abandoned at an early, but promising, state of development. Basic feasibility is established, but much more remains to be done.

The short-term objectives include:

1) Replacement of the simulated target by a photoconductor.

2) Better resolution and larger size of the image.

3) Correction of edge distortion and ellipticity.

The long-term objectives may include:

4) Increase of voltage-control sensitivity by one order of magnitude.

5) Control over the polarity of the reflected electron image.

6) Introduction of a charge-storing target before display.

Items 4) and 5) may well be solved in combination by the introduction of "dark field" types of electron-optics, similar to "Schlieren" techniques as used in light optics. Item 6) may require the use of time-sharing operations, including display by recurrent pulses.

9. FUTURE DEVELOPMENTS AND RECOMMENDATIONS (Continued)

The finished image converter with photoconductive target may prove to be a very useful device for the direct viewing of thermal images. Its sensitivity may never be a match for scanning types of IR-pickup tubes. However, due to the absence of a camera chain, the entire equipment is much simpler. The Thermal Image Converter will be portable complete with its power supply. It may find its own particular applications in the industrial and military domain.

LITERATURE REFERENCES

1. G. Holst, H. J. deBoer, M. C. Teves, C. F. Veenermans

"An Apparatus for the Transformation of Light of Long Wavelength into Light of Short Wavelength", Physics, Vol. 1, pp 297-305, 1934.

2. V. K. Zworykin and G. A. Morton

"Applied Electron Optics", J. Optical Soc. Am., Vol 26, pp 181-189, 1936.

3. G. A. Morton and E. G. Ramberg

"Electron Optics of an Image Tube", Physics, Vol. 7, pp 451-459, 1936.

4. G. A. Morton and L. E. Flory

"Infrared Image Tube", Electronics, Vol. 19, pp 112-114, September 1946.

5. V. K. Zworykin and E. G. Ramberg

"Photoelectricity", J. Wiley, 4th printing, 1961 Chapter 9, pp 155-174.

6. P. Schagen, H. Bruining, and J. C. Francken

"A Simple Electrostatic Electron-Opticsl System With Only One Votlage", Philips Research Reports, Vol. 7, pp 119-130, April 1952.

7. See, for instance:

Monovoltage-type Image Converter Tube RCA #6914.

8. J. C. Francken and H. Bruining

"New Developments in the Image Iconoscope", Philips Technical Review, Vol. 14, No. 11, pp 327-335, May 1953.

9. J. A. Jenkins and R. A. Chippendale

"High Speed Photography by Means of the Image Converter", Philips Technical Review, Vol. 14, No. 8, pp 213-244, February 1953.

LITERATURE REFERENCES (Continued)

10. B. R. Linden and P. A. Snell

"Shutter Image Converter Tubes", Proceedings I.R.E., Vol. 45, No. 4, pp 513-523, April 1957.

11. J. C. Francken and R. Dorrestein

"Paraxial Image Formation in the Magnetic Image Iconoscope" Philips Res. Reports, Vol. 6, pp 323-346, 1951 (No. 5).

12. P. Schagen

"An Image Tube With Built-In Electrostatic Zoom Lens" Lecture, October 25, 1962, IRE Electron Devices Meeting Washington, D.C.

13. H. Baker and G. Papp

"Magnetically Focused Image Converter Tubes", Lecture, Image Intensifier Symposium, Ft. Belvoir, Virginia October 6-7, 1958.

14. V. K. Zworykin and E. G. Ramberg

"Photoelectricity", 4th Printing, John Wiley & Sons, New York, 1961, p 170, Figure 9.13.

15. G. A. Morton and E. G. Ramberg

"Electron Optics of an Image Tube", Physics, Vol. 7, 1936, pp 451-459.

16 ITT Industrial Laboratories, Components and Instrumentation Department, Fort Wayne, Indiana

"Application Notes on Type 7177/1C-6 and 6411/1C-16-3"

17. V. K. Zworykin and G. A. Morton

"Television", Second Edition, John Wiley and Sons, New York, 1954, Chapter 3, Section 3.5, pp 105-108.

18. V. E. Cosslet

"Electron Optics", Second Edition-Oxford Clarendon Press, 1950, Section 16, p 30.

LITERATURE REFERENCES (Continued)

19. K. Schlesinger

"Electron Trigonometry, a New Tool for Electron-Optical Design", Proceedings I.R.E., Vol. 49, No. 10, October 1961, pp 1538-1549.

20. P. Schagen, H. Bruining, J. C. Francken

"A Simple Electrostatic Electron-Optical System With Only One Voltage", Philips Research Reports, Vol. 7, April 1962 pp 119-130.

21. B. R. Linden and P. A. Snell

"Shutter Image Converter Tubes", Proceedings of the I.R.E., Vol. 45, No. 4, April 1957, pp 513-523, Figure 8.

22. Charles D. Hodgman

"CFC Standard Mathematical Tables", Twelfth Edition, Fourth Printing, Chemical Rubber Publishing Co., Cleveland, Ohio, March 1961, p 419, Figure 6.

23. Jenkins and White

"Fundamentals of Optics", Section 9.11, Figure 9U, pp 152-154, Third Edition, McGraw Hill, 1957.

24. Kruse, McGlauchlin, and McQuistan

"Elements of Infrared Technology" Wiley, 1962, pp 408-409; also Table 10.1, p 421.

25. K. Schlesinger (D. G. Fink, ed.)

"Television Engineering", McGraw Hill, First Edition, 1957 Section 6-3, Figure 6-2, eq. 6.6.

DISTRIBUTION LIST

Cys	ACTIVITIES AT WPAFB
6 + repro	ASD (ASRNE-42) Wright-Patterson AFB Ohio
1	ASD (ASAPR) (OTS Review) Wright-Patterson AFB Ohio
1	ASD (ASAPRL) Wright-Patterson AFB Ohio
3	ASD (ASAPT) Wright-Patterson AFB Ohio
1	ASD (ASRNRS-31) Wright-Patterson AFB Ohio
1	ASD (ASRNRS-13) Wright-Patterson AFB Ohio
	OTHER DEPARTMENT OF DEFENSE ACTIVITIES
	Air Force
1	RADC (RCSGA) Attn: Mr. Kesselman Griffiss AFB NY
1	ESD (ESRDE) Attn: Maj Van Horn L G Hanscom Fld Bedford, Mass
	Army
1	Commanding Officer USAERDL Attn: SELRA-PRG Mr. M. E. Crost Ft. Monmouth, New Jersey
1	Commanding General USAERDL Attn: Warfare Vfsion Branch Ft. Belvoir, Virginia
1	Commanding Officer USAERDL Attn: Technical Documents Center Evans Signal Lab Area, Bldg. 27 Belmar, New Jersey

Cys	Army (Continued)
1	Commander Army Rocket & Guided Missile Agency, Attn: Technical Library, ORDXR-OTL Redstone Arsenal, Alabama
1	Commanding Officer Attn: ORDTL-012 Diamond Ordnance Fuze Labs. Wash 25, D. C.
	Navy
1	Chief Bureau of Ships Attn: Mrs. F.R. Darne, Code 691A Wash 25, D. C.
1	Chief Naval Research Laboratory Building 33, Room 118 Wash 25, D. C.
1	Naval Ordnance Test Station Attn: Mr. J. Rughe 1207 Michelson Laboratory China Lake, California
1	New York Naval Shipyard (911b) Brooklyn 1, New York
1	Commanding Officer U.S. Naval Ordnance Laboratory Corona, California
	OTHER US GOVERNMENT AGENCIES
30	ASTIA (TIPCR) Arlington Hall Stn Arlington 12, Va
4	Advisory Group on Electronic Devices Attn: Secretary, Working Group on Special Devices 346 Broadway, 8th Floor New York 13, New York
1	National Bureau of Standards Electricity & Electronics Div. Engineering Electronics Section Attn: Mr. Gustave Shapiro Wash 25, D. C.

Cys	OTHER US GOVERNMENT AGENCIES (Contd)
100	OTS, Stock 1200 Eads Street Arlington, Va.

NON-GOVERNMENT INDIVIDUALS AND ORGANIZATIONS

Cys	
1	Philco Corporation Attn: Mr. Charles Comeau Tioga and C Streets Philadelphia, Pennsylvania
20	General Electric Company Cathode Ray Tube Department Attn: Dr. Schlesinger Electronics Park Syracuse, New York
1	Westinghouse Electric Corporation Electron Tube Division Attn: Dr. Hilary Moss Elmira, New York
3	Radio Corporation of America Attn: Mr. G. W. Kimball 224 North Wilkinson Street Dayton 2, Ohio
1	The Rand Corporation Attn: Librarian 1700 Main Street Santa Monica, California
1	General Electrodynamics Corporation 4430 Forest Lane Garland, Texas
1	ITT Industrial Laboratories Attn: Mr. Eberhardt 3700 East Pontiac Street Fort Wayne 1, Indiana
1	Hughes Research Laboratories Attn: Mr. Norman Lehrer Special Tubes Section 3011 Malibu Road Malibu, California

Cys	NON-GOVERNMENT INDIVIDUALS AND ORGANIZATIONS
1	Field Emission Corporation Attn: Mr. F.M. Charbonnier 611 Third Street McMinnville, Oregon
1	CBS Laboratories High Ridge Road Stamford, Connecticut
1	Sanders Associates, Inc. Attn: Norman Wild Nashua, New Hampshire
1	A.B. DuMont Labs. Div. of Fairchild Camera & Inst. Corporation 750 Bloofield Ave. Clifton, N. J.
1	Litton Industries Electron Tube Division Attn: Dr. Porkorny 960 Industrial Road San Carlos, California

Aeronautical Systems Division,Air Force Avionics Lab,Electronic Technology Div,Wright-Patterson AFB,Ohio Rpt No. ASD-TDR-63-461,STUDY OF ELECTRON FOCUSING BY NON-LINEAR SPIRALS. Final report,May 63, 98 p incl illus, tables, 25 refs.

Unclassified Report

An electrostatic image converter has been developed. Its capabilities include: plane-to-plane image formation; magnification control over a 4-to-1 range; separate control of image intensity; stop-motion operation by a built-in shutter grid. The use of a planar cathode has become practical, due to a built-in field-flattener, using an internal mesh of hyperconvex shape. Zoom-lens action has been accomplished by a system of two spiral lenses, used in tandem as either

UNCLASSIFIED

1. Cathode-ray tubes
2. Electron beams
3. Focusing
4. Image tubes
5. Electron optics

I. Project 4156, Task 415605
II. AF33(657)-7682
III. General Electric Co.,Syracuse, N.Y.
IV. Schlesinger,K.
V. C59R-2M-FR
VI. In ASTIA coll.

UNCLASSIFIED

Aeronautical Systems Division, Air Force Avionics Lab,Electronic Technology Div,Wright-Patterson AFB,Ohio Rpt No. ASD-TDR-63-461,STUDY OF ELECTRON FOCUSING BY NON-LINEAR SPIRALS. Final report,May 63, 98 p incl illus, tables, 25 refs.

Unclassified Report

An electrostatic image converter has been developed. Its capabilities include: plane-to-plane image formation; magnification control over a 4-to-1 range; separate control of image intensity; stop-motion operation by a built-in shutter grid. The use of a planar cathode has become practical due to a built-in field-flattener using an internal mesh of hyperconvex shape. Zoom-lens action has been accomplished by a system of two spiral lenses, used in tandem as either

UNCLASSIFIED

1. Cathode-ray tubes
2. Electron beams
3. Focusing
4. Image tubes
5. Electron optics

I. Project 4156 Task 415605
II. AF33(657)-7682
III. General Electric Co.,Syracuse, N.Y.
IV. Schlesinger,K.
V. C59R-2M-FR
VI. In ASTIA collection

UNCLASSIFIED

Aeronautical Systems Division,Air Force Avionics Lab, Electronic Technology Div,Wright-Patterson AFB,Ohio Rpt No. ASD-TDR-63-461,STUDY OF ELECTRON FOCUSING BY NON-LINEAR SPIRALS. Final report,May 63, 98 p incl illus, tables, 25 refs.

Unclassified Report

An electrostatic image converter has been developed. Its capabilities include: plane-to-plane image formation; range; separate control of image intensity; stop-motion operation by a built-in shutter grid. The use of a planar cathode has become practical, due to a built-in field-flattener, using an internal mesh of hyperconvex shape. Zoom-lens action has been accomplished by a system of two spiral lenses, used in tandem as either

UNCLASSIFIED

1. Cathode-ray tubes
2. Electron Beams
3. Focusing
4. Image tubes
5. Electron optics

I. Project 4156, Task 415605
II. AF33(657)-7682
III. General Electric Co.,Syracuse, N.Y.
IV. Schlesinger,K.
V. C59R-2M-FR
VI. In ASTIA coll.

UNCLASSIFIED

Aeronautical Systems Division, Air Force Avionics Lab,Electronic Technology Div,Wright-Patterson AFB,Ohio Rpt.No. ASD-TDR-63-461,STUDY OF ELECTRON FOCUSING BY NON-LINEAR SPIRALS. Final report,May 63,98 p incl illus., tables, 25 refs.

Unclassified Report

An electrostatic image converter has been developed. Its capabilities include: plane-to-plane image formation; range; separate control of image intensity; stop-motion operation by a built-in shutter grid. The use of a planar cathode has become practical, due to a built-in field-flattener, using an internal mesh of hyperconvex shape. Zoom-lens action has been accomplished by a system of two spiral lenses, used in tandem as either

UNCLASSIFIED

1. Cathode-ray tubes
2. Electron beams
3. Focusing
4. Image tubes
5. Electron optics

I. Project 4156 Task 415605
II. AF33(657)-7682
III. General Electric Co.,Syracuse, N.Y.
IV. Schlesinger,K.
V. C59R-2M-FR
VI. In ASTIA collection

UNCLASSIFIED

positive or negative elements. All tubes reported use strong acceleration by a plane anode-mesh near cathode. A concluding section deals with image formation from photoconductive targets, done by means of re flective electron optics, using a collimated, but non-scanning, flood-beam for target illumination. Preliminary experiments with a simulated target gave images with fair resolution (30 l.p.i.), fully modulated by a charge distribution on target equivalent to a 30-volt range of surface potential. Unclassified abstract	UNCLASSIFIED UNCLASSIFIED	positive or negative elements. All tubes reported use strong acceleration by a plane anode-mesh near cathode. A concluding section deals with image formation from photoconductive targets, done by means of reflective electron optics, using a collimated, but non-scanning, flood-beam for target illumination. Preliminary experiments with a simulated target gave images with fair resolution (30 1.p.i.), fully modulated by a charge distribution on target equivalent to a 30-volt range of surface potential. Unclassified abstract	UNCLASSIFIED UNCLASSIFIED
positive or negative elements. All tubes reported use strong acceleration by a plane anode-mesh near cathode. A concluding section deals with image formation from photoconductive targets, done by means of re flective electron optics, using a collimated, but non-scanning, flood-beam for target illumination. Preliminary experiments with a simulated target gave images with fair resolution (30 1.p.i.), fully modulated by a charge distribution on target equivalent to a 30-volt range of surface potential. Unclassified Abstract	UNCLASSIFIED UNCLASSIFIED	positive or negative elements. All tubes reported use strong acceleration by a plane anode-mesh near cathode. A concluding section deals with image formation from photoconductive targets, done by means of reflective electron optics, using a collimated, but non-scanning, flood-beam for target illumination. Preliminary experiments with a simulated target gave images with fair resolution (30 1.p.i.), fully modulated by a charge distribution on target equivalent to a 30-volt range of surface potential. Unclassified Abstract	UNCLASSIFIED UNCLASSIFIED

FOR ERRATA

AD_____

414486

THE FOLLOWING PAGES ARE CHANGES

TO BASIC DOCUMENT

GENERAL ELECTRIC COMPANY

POWER TUBE DEPARTMENT

ELECTRONICS PARK, SYRACUSE, N. Y. . . . TEL. AREA 315 . . . DIAL 456 Plus EXT.*

PICKUP TUBE OPERATION

Bldg. 6 - Electronics Park
Syracuse, New York

AD 414 486

Re: ASD-TDR-63-461, Final Report, AF 33(657)-7682

Please replace Figures 3.13 (page 51) and 6.3 (page 84) in the subject report with the respective figures attached. These new figures are of better quality than the originals in the report.

L M Strom

L. M. Strom, Specialist
Contract Administration

LMS:bw
Ext. 2945

Att.

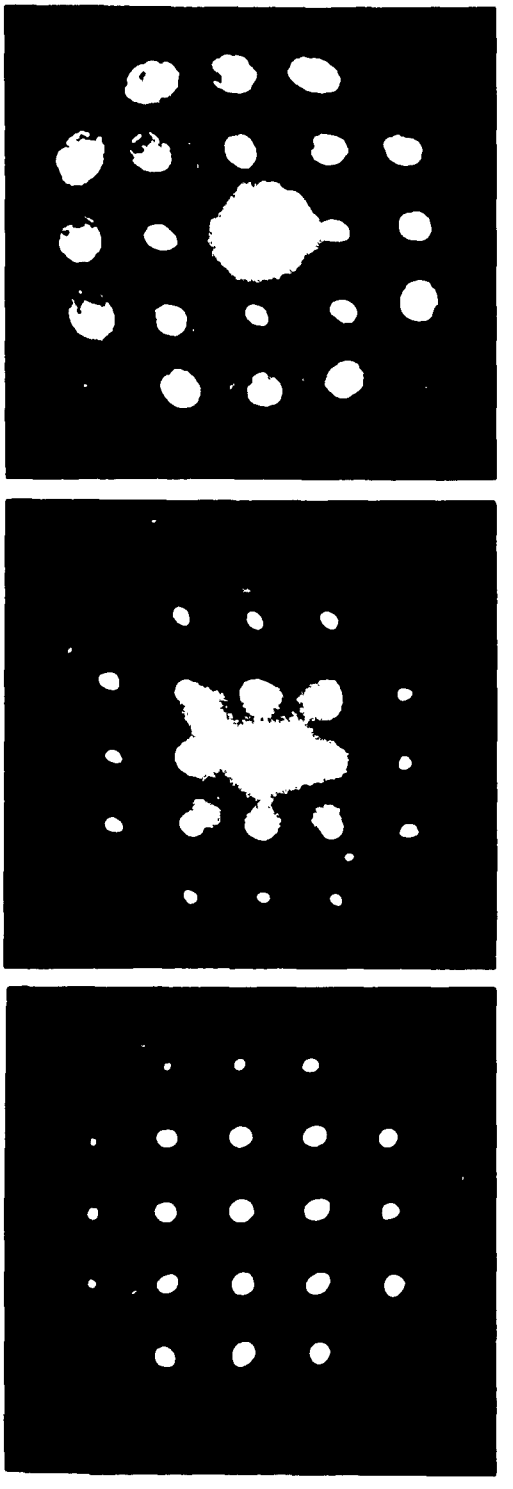

a.

b.

c.

Figure 3.13- Correction for Curvature of **Field**

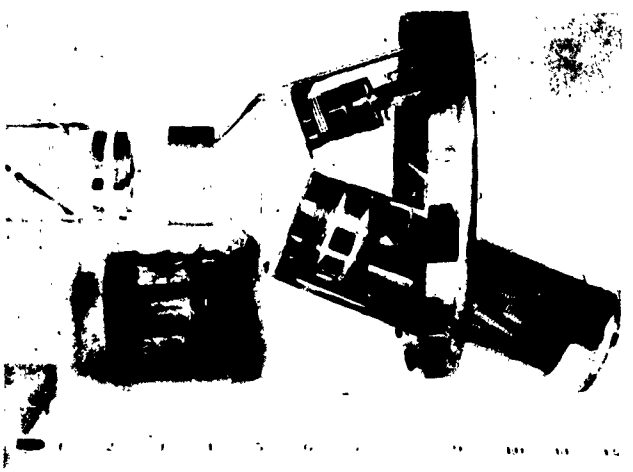

Fig. 6.3- REFLECTIVE OPTICS WITH INCLINED GUNS

GENERAL ELECTRIC COMPANY

ELECTRONICS PARK, SYRACUSE, N. Y. 13201 . . . TEL. AREA 315 . . . DIAL 456 Plus EXT.*

TUBE DEPARTMENT

SYRACUSE
PICKUP TUBE OPERATION

Bldg. 6 - Electronics Park
Syracuse, New York
November 18, 1963

MEMO

Subject: ASD-TDR-63-461
Final Report
Contract # AF 33(657)-7682

Please substitute the attached figure for Figure 3.13, page 51, in your copy of the subject report.

Very truly yours,

L. M. Strom/bw

L. M. Strom, Specialist
Contract Administration

bw
Ext. 2945

Att.

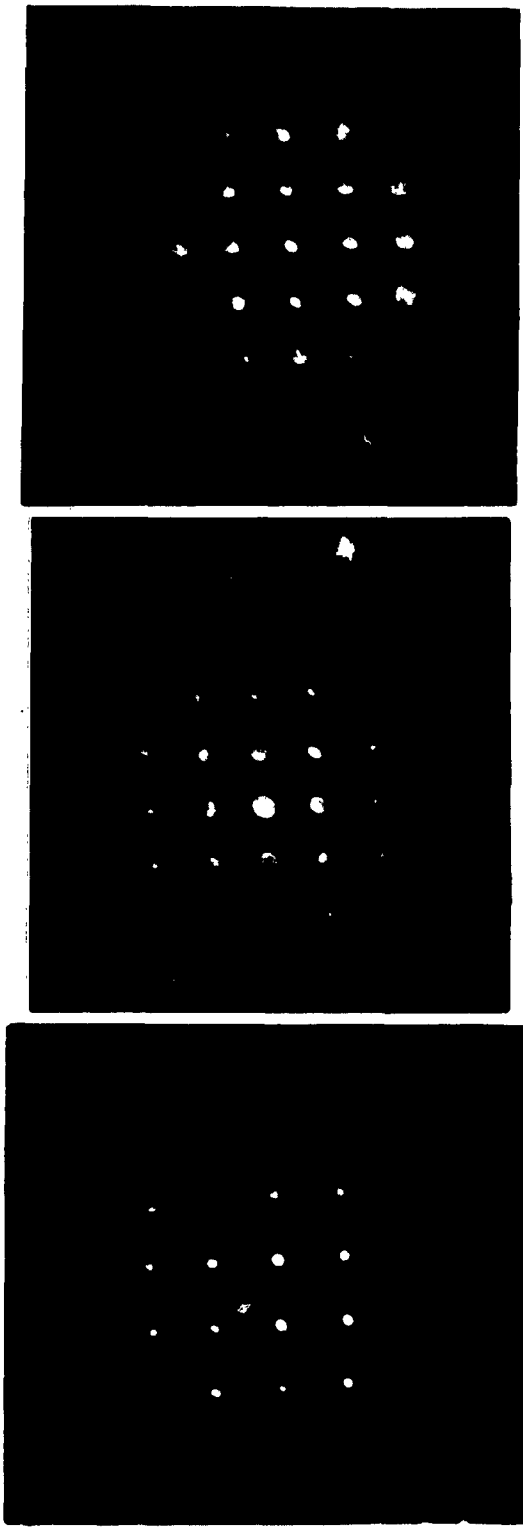

a.

b.

c.

Figure 3.13- Correction for Curvature of Field

AD_____

414486

END CHANGE PAGES